

Modularity in Multilayer Networks using Redundancy-based Resolution and Projection-based Inter-Layer Coupling[‡]

Alessia Amelio¹, Giuseppe Mangioni², and Andrea Tagarelli^{‡1}

¹Dept. of Computer Engineering, Modeling, Electronics and Systems Engineering (DIMES),
University of Calabria, Rende (CS), Italy, Email: {aamelio, tagarelli}@dimes.unical.it.

²Dept. of Electrical, Electronics and Computer Engineering, University of Catania, Catania,
Italy, Email: giuseppe.mangioni@dieei.unict.it.

Abstract

The generalized version of modularity for multilayer networks, a.k.a. multislice modularity, is characterized by two model parameters, namely resolution factor and inter-layer coupling factor. The former corresponds to a notion of layer-specific relevance, whereas the inter-layer coupling factor represents the strength of node connections across the network layers. Despite the potential of this approach, the setting of both parameters can be arbitrarily selected, without considering specific characteristics from the topology of the multilayer network as well as from an available community structure. Also, the multislice modularity is not designed to explicitly model order relations over the layers, which is of prior importance for dynamic networks.

This paper aims to overcome the main limitations of the multislice modularity by introducing a new formulation of modularity for multilayer networks. We revise the role and semantics of both the resolution and inter-layer coupling factors based on information available from the within-layer and inter-layer structures of the multilayer communities. Also, our proposed multilayer modularity is general enough to consider orderings of network layers and their constraints on layer coupling. Experiments were carried out on synthetic and real-world multilayer networks using state-of-the-art approaches for multilayer community detection. The obtained results have shown the meaningfulness of the proposed modularity, revealing the effects of different combinations of the resolution and inter-layer coupling functions. This work also represents a starting point for the development of new optimization methods for community detection in multilayer networks.

*Accepted for publication with *IEEE Trans. on Network Science and Engineering*, April 2019. DOI: 10.1109/TNSE.2019.2913325

[†]An abridged version of this work appeared in [1].

[‡]Corresponding author: Andrea Tagarelli.

1 Introduction

Complex network systems, such as social networks, biological networks, and transportation networks, are inherently organized into *communities*, a.k.a. clusters or modules, with dense internal links and sparse external links. Since members of a community tend to generally share common properties, revealing the community structure in a network can provide a better understanding of the overall functioning of the network.

The well-known *modularity* [2, 3] function was originally conceived to evaluate a community structure in a network graph in terms of difference between the actual number of edges linking nodes inside each community and the expected connectivity in the null model. Typically, the expected connectivity is expressed through a configuration graph model, having a certain degree distribution and randomized edges. Since this graph ignores any community structure, a large difference between actual connectivity and expected connectivity would indicate the presence of a community structure.

Modularity has been widely utilized as objective function in several optimization methods designed for discovering communities in networks [4, 5], including greedy agglomeration [3, 6], spectral division [7, 8], simulated annealing [9], or extremal optimization [10].

Traditional approach to network analysis refers to the modeling of a real-world system as a single network of interacting entities. While this approach has been widely used to study a variety of applications, there are plenty of scenarios for which this methodology appears strongly limiting [11]. In general, ties among entities could be induced by one or several types of relations or interactions, or even be dependent on side-information based on specific dimensions or aspects of interest for the entities in the network. Within this view, *multilayer networks* [12, 13] represent a powerful tool to model systems interconnected by multiple types of relations. In the multilayer network model, each type of connection is represented by a layer, and an entity may be present in different layers based on the type of relations it is connected to its neighbor entities. Just to mention one real example, nowadays online users usually have multiple accounts across different online social networks, and several online/offline relationships are likely to occur among the same group of individuals (e.g., following relations, like/comment interactions, working together, having lunch). It should be emphasized that neglecting such a kind of complex organization by reducing the whole system to a single network (e.g., through some kind of projection, or by aggregation), has been shown to be much less informative than the multilayer representation [14]. For the above mentioned reasons, multilayer networks are experiencing an increasing interest from the scientific community, leading to an explosion of scientific papers in many areas of science, thus becoming one of the most used tools for interdisciplinary research [15], [16], [11], [13], [17], [18], [12], [19], [20, 21], [22], [23].

Clearly, the problem of community detection in such multilayer networks takes a central role to unveil meaningful patterns of node groupings into communities, by leveraging the various interaction modes that involve all the entity

nodes in the network. To address these needs, modularity has been extended to the general case of multilayer networks. In particular, Mucha et al. [15] extend the modularity function to arbitrary multilayer networks (also called *multislice* in that work), by introducing two additional parameters w.r.t. classic modularity: a *resolution* parameter and an *inter-layer coupling* factor. The resolution parameter acts on the expected connectivity terms, thus controlling the effect on the size distribution of community due to the *resolution limit* known in modularity [24]. The inter-layer coupling factor focuses on the links across layers and hence impacts on the strength of the inter-layer connections of entities in the network. While being important to enhance the ability of modularity in evaluating a community structure, the two parameters introduced in the multislice modularity are nonetheless subjected to arbitrary choices, which raise a number of issues in the application of this modularity function. In particular, the resolution parameter can be arbitrarily set for each layer, but it discards any structure information at graph or community level. Moreover, the inter-layer coupling terms do not differentiate among the selected layers, and all pairs of layers can in principle be considered, which makes no sense in certain scenarios such as modeling of time-evolving networks.

The above considerations prompted us to revisit the notion of modularity in multilayer networks, and in particular to introduce novel aspects to take into account in both the resolution and inter-layer coupling definitions. First, the layer-specific resolution factor is also made dependent on each particular community. We notice that, since a high-quality multilayer community should embed high information content among its nodes, the resolution of a specific layer to control the expected connectivity of a given community in the modularity function should be lower as the contribution of that layer to the information content of the community is higher. By relating the information content of a multilayer community to the amount and variety of types of links internal to the community, we provide a new definition of resolution factor based on the concept of *redundancy* of community. Second, to determine the strength of coupling of nodes across layers, we again consider it at community level, such that for each pair of layers, the inter-layer coupling factor for nodes in a community depends on the relevance of the community projection on the two layers. Moreover, we account for an available *ordering of the layers*, and relating constraints on their coupling validity.

Our main contributions are summarized as follows:

- We propose a novel definition of multilayer modularity, in which we reconsider the role and semantics of its two key terms, that is, the resolution factor and inter-layer coupling factor. We conceive parameter-free unsupervised approaches for their computation, which leverage information from the within-layer and across-layer structures of the communities in the multilayer network. Moreover, our formulation of multilayer modularity is general enough to account for an available ordering of the layers, therefore is also well-suited to deal with temporal multilayer networks.
- We provide theoretical insights into properties of the proposed multilayer

modularity. More specifically, we investigate the effect of increasing the number of communities in the behavior of the multilayer modularity, and we analytically derive the lower and upper bounds in the values of the multilayer modularity.

- We conduct an extensive experimental evaluation, primarily to understand how the proposed multilayer modularity behaves w.r.t. different settings regarding the resolution and the inter-layer coupling terms. Using 4 state-of-the-art methods for multilayer community detection (GL, PMM, LART, and M-EMCD*), LFR synthetic multilayer networks and 10 real-world multilayer networks, results have shown the significance of our formulation and the different expressiveness against the previously existing multislice modularity.

2 Related Work

Community detection is a key-enabling task in network analysis and mining, with tons of methods developed in the last ten years — please refer to [25, 26, 16, 27] for surveys on this topic. In addition, different metrics for community structure evaluation have been introduced. As discussed in Section 1, the most popular and widely accepted measure is the so-called “modularity”, defined by Newman [2]. Initially conceived for undirected networks, the modularity function has been subsequently extended to cover different cases. In [28][29], modularity has been generalized to directed networks incorporating information contained in edge directions, while in [30] modularity is also adapted to capture communities in weighted networks. To overcome the well-known modularity resolution limit [24, 31, 32], in [33] and [34] modularity has been modified by incorporating a resolution parameter that helps reveal communities at different resolution scale. A further step towards a generalization of the modularity refers to its extension to signed networks [35, 36]. Also, to deal with bipartite networks, modifications have been proposed in [37, 38, 39]. To uncover overlapping communities, in [40] the authors propose an extension to the modularity function that includes the notion of belonging (or membership) coefficient, which measures to which extent a node belongs to the various communities. This approach is sometimes referred to as fuzzy community discovering. Finally, as introduced in Section 1, modularity has been generalized by [15] to capture communities in multislice networks. Such a version of the modularity function is detailed in the next section.

3 Background

3.1 Modularity

Given an undirected graph $G = (\mathcal{V}, \mathcal{E})$, with $n = |\mathcal{V}|$ nodes and $m = |\mathcal{E}|$ edges, let \mathcal{C} be a community structure over G . For any $v \in \mathcal{V}$, we use $d(v)$ to denote the

degree of v , and for any community $C \in \mathcal{C}$, symbol $d(C)$ to denote the degree of C , i.e., $d(C) = \sum_{v \in C} d(v)$; also, the total degree of nodes over the entire graph, $d(\mathcal{V})$, is defined as $d(\mathcal{V}) = \sum_{v \in \mathcal{V}} d(v) = \sum_{C \in \mathcal{C}} d(C) = 2m$. Moreover, we denote with $d_{int}(C)$ the internal degree of C , i.e., the portion of $d(C)$ that corresponds to the number of edges linking nodes in C to other nodes in C . Newman and Girvan's *modularity* is defined as follows [2]:

$$Q_{NG}(\mathcal{C}) = \sum_{C \in \mathcal{C}} \frac{d_{int}(C)}{d(\mathcal{V})} - \left(\frac{d(C)}{d(\mathcal{V})} \right)^2 \quad (1)$$

In the above equation, the first term is maximized when many edges are contained in clusters, whereas the second term is minimized by partitioning the graph into many clusters with small total degrees. The value of Q_{NG} ranges within -0.5 and 1.0 [4]; it is minimum for any bipartite network with canonic clustering, and maximum when the network is composed by disjoint cliques.

3.2 Multilayer network model

Let $G_{\mathcal{L}} = (V_{\mathcal{L}}, E_{\mathcal{L}}, \mathcal{V}, \mathcal{L})$ be a *multilayer network* graph, where \mathcal{V} is a set of entities and $\mathcal{L} = \{L_1, \dots, L_\ell\}$ is a set of layers. Each layer represents a specific type of relation between entity nodes. Let $V_{\mathcal{L}} \subseteq \mathcal{V} \times \mathcal{L}$ be the set containing the entity-layer combinations, i.e., the occurrences of each entity in the layers. $E_{\mathcal{L}} \subseteq V_{\mathcal{L}} \times V_{\mathcal{L}}$ is the set of undirected links connecting the entity-layer elements. For every $L_i \in \mathcal{L}$, we define $V_i = \{v \in \mathcal{V} \mid (v, L_i) \in V_{\mathcal{L}}\} \subseteq \mathcal{V}$ as the set of nodes in the graph of L_i , and $E_i \subseteq V_i \times V_i$ as the set of edges in L_i . Each entity must be present in at least one layer, i.e., $\bigcup_{i=1..l} V_i = \mathcal{V}$, but each layer is not required to contain all elements of \mathcal{V} . We assume that the inter-layer links only connect the same entity in different layers, however each entity in one layer could be linked to the same entity in a few or all other layers.

3.3 Multislice Modularity

Given a community structure \mathcal{C} identified over a multilayer network $G_{\mathcal{L}}$, the *multislice modularity* [15] of \mathcal{C} is defined as:

$$\begin{aligned} Q_{ms}(\mathcal{C}) &= \frac{1}{d(V_{\mathcal{L}})} \sum_{\substack{u,v, \\ L_i, L_j}} \left[\left(A_{uvL_i} - \gamma_i \frac{d_{L_i}(u)d_{L_i}(v)}{2|E_i|} \right) \times \right. \\ &\quad \left. \times \delta_{L_i, L_j} + \delta_{u,v} C_{v, L_i, L_j} \right] \delta(g_{u, L_i}, g_{v, L_j}) \end{aligned} \quad (2)$$

where $d(V_{\mathcal{L}})$ is the total degree of the multilayer network graph, $d_{L_i}(u)$ denotes the degree of node u in layer L_i , A_{uvL_i} denotes a link between u and v in L_i , $2|E_i|$ is the total degree of the graph of layer L_i , γ_i is the resolution parameter for layer L_i , C_{v, L_i, L_j} quantifies the links of node v across layers L_i, L_j . Moreover, the Dirichlet terms have the following meanings: δ_{L_i, L_j} is equal to 1 if $L_i = L_j$ and 0 otherwise, $\delta_{u,v}$ is equal to 1 if $u = v$ and 0 otherwise (i.e., the inter-layer coupling is allowed only for nodes corresponding to the same entity), and

$\delta(g_{u,L_i}, g_{v,L_j})$ is equal to 1 if the community assignments of node u in L_i and node v in L_j are the same and 0 otherwise.

Limitations of Q_{ms} . As previously mentioned, a different resolution parameter γ_i can be associated with each layer to express its relevance weight; however, in [15], there is no specification of any principled way to set a layer-weighting scheme, possibly including information from the available multilayer community structure. Moreover, neither the inter-layer coupling term (i.e., C_{v,L_i,L_j}) or any constraint on the layer comparability are clearly defined; actually, all nonzero inter-layer edges are set to a constant value ω , for all unordered pairs of layers. In general, both γ_i and ω parameters can assume any non-negative value, which further increases a clarity issue in the properties of Q_{ms} .

4 Proposed Multilayer Modularity

In this section, we propose a new definition of modularity for multilayer networks that aims to overcome all of the issues of Q_{ms} previously discussed. We pursue this goal by focusing on the role and semantics of the two key elements in multilayer modularity: the *layer-specific resolution* and the *inter-layer coupling*.

Our definitions of the two terms are independent on a-priori assumptions on the network and/or user-specified settings; by contrast, we conceive parameter-free unsupervised approaches for their computation, by leveraging information from the within-layer and inter-layer structures of the communities. Our proposed resolution factor is computed for pairs of layer and community, rather than for each layer globally. Analogously, to define the inter-layer coupling term, we account for properties related to a community on two layers; more in detail, we evaluate the projections of a community over any two comparable layers, i.e., the sets of nodes belonging to a community that lay on those layers. Remarkably, the comparability of layers is another key aspect of our definition of modularity: we generalize the inter-layer coupling term by admitting the existence of a *partial order relation* $\prec_{\mathcal{L}}$ over the layers, in order to properly represent scenarios in which a particular ordering among layers is required. For instance, it may be the case that the network layers have to be processed according to their natural order (e.g., lexicographic order of the network labels), or according to a temporal order; moreover, it may be required to compare adjacent layers only, or each layer with any other succeeding it in the ordering. Figure 1 provides an illustration of a multilayer network and the aforementioned key aspects we deal with in our proposed multilayer modularity, which is formally presented next.

Definition 4.1 (Multilayer Modularity). *Let $G_{\mathcal{L}} = (V_{\mathcal{L}}, E_{\mathcal{L}}, \mathcal{V}, \mathcal{L})$ be a multilayer network graph, and let $\prec_{\mathcal{L}}$ be an optionally provided partial order relation over the set of layers \mathcal{L} . Given a community structure $\mathcal{C} = \{C_1, \dots, C_k\}$ as a*

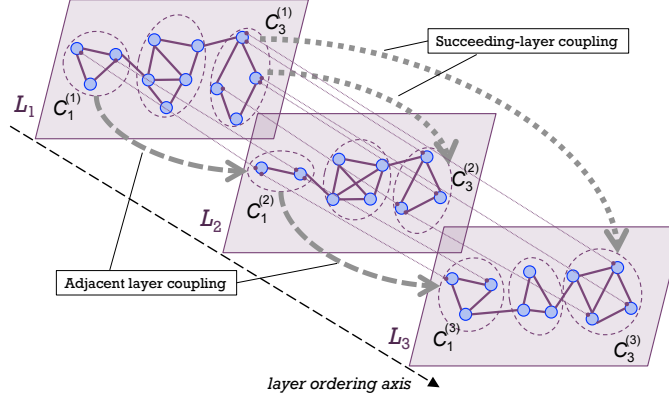


Figure 1: Example multilayer network. The ordering over the set of layers enables the introduction of constraints to compare layers; for instance, adjacent-layer coupling forces the comparison of adjacent layers only, while succeeding-layer coupling allows each layer to be compared with the subsequent ones. Note also that any community across the layers is visually represented by means of each projection from one layer to another valid layer; for instance, using succeeding-layer coupling, community C_3 in layer L_1 is projected onto layer L_2 and layer L_3 .

partitioning of the multilayer graph $G_{\mathcal{L}}$, the multilayer modularity is defined as:

$$Q(\mathcal{C}) = \frac{1}{d(V_{\mathcal{L}})} \sum_{C \in \mathcal{C}} \left[\sum_{L \in \mathcal{L}} \left(d_L^{int}(C) - \gamma(L, C) \frac{(d_L(C))^2}{d(V_{\mathcal{L}})} + \beta \sum_{L' \in \mathcal{P}(L)} IC(C, L, L') \right) \right] \quad (3)$$

where for any $C \in \mathcal{C}$ and $L \in \mathcal{L}$:

- $d_L(C)$ and $d_L^{int}(C)$ are the degree of C and the internal degree of C , respectively, by considering only edges of layer L ;
- $\gamma(L, C)$ is the value of the resolution function;
- $IC(C, L, L')$ is the value of the inter-layer coupling function for any valid layer pairings with L ;
- $\beta \in \{0, 1\}$ is a parameter to control the exclusion /inclusion of inter-layer couplings; and
- $\mathcal{P}(L)$ is the set of valid pairings with L defined as:

$$\mathcal{P}(L) = \begin{cases} \{L' \in \mathcal{L} \mid L \prec_{\mathcal{L}} L'\}, & \text{if } \prec_{\mathcal{L}} \text{ is defined} \\ \mathcal{L} \setminus \{L\}, & \text{otherwise} \end{cases}$$

□

Notably, unlike the multislice modularity in Eq. (2), our proposed modularity originally introduces a resolution factor that varies with each community, and an inter-layer coupling scheme that might also depend on the layer ordering. Moreover, Eq. (3) utilizes the total degree $d(V_{\mathcal{L}})$ of the multilayer graph instead of the layer-specific degree (i.e., term $2|E_{L_i}|$, for each $L_i \in \mathcal{L}$). The latter difference w.r.t. the multislice modularity is also important because, as we shall later discuss more in detail, the total degree of the multilayer graph includes the inter-layer couplings and it might be defined in different ways depending on the scheme of inter-layer coupling. In the following, we elaborate on the resolution functional term, $\gamma(\cdot, \cdot)$, and the inter-layer coupling functional term, $IC(\cdot, \cdot, \cdot)$.

4.1 Redundancy-based resolution factor

The layer-specific resolution factor intuitively expresses the relevance of a particular layer to the calculation of the expected community connectivity in that layer. While this can always reflect some predetermined scheme of relevance weighting of layers, we propose a more general definition that accounts for the strength of the contribution that a layer takes in determining the internal connectivity for each community. The key assumption underlying our approach is that, since a high quality community should envelope high information content among its elements, *the resolution of a layer to control the expected connectivity of a given community should be lowered as the layer’s contribution to the information content of the community increases.*

In this regard, the *redundancy* measure proposed in [41] is particularly suited to quantify the variety of connections, such that it is higher if edges of more types (layers) connect each pair of nodes in the community. Let us denote with P_1 the set of node pairs connected in at least one layer in the graph, and with P_2 the set of “redundant” pairs, i.e., the pairs of nodes connected in at least two layers. Given a community C , P_1^C and P_2^C denote the subset of P_1 and the subset of P_2 , respectively, corresponding to nodes in C . The redundancy of C , $\rho(C)$, expresses the number of pairs in C with redundant connections, divided by the number of layers connecting the pairs. Formally [41]:

$$\rho(C) = \sum_{(v,u) \in P_2^C} \frac{SL(v,u,\mathcal{L})}{|\mathcal{L}| \times |P_1^C|}, \quad (4)$$

with $SL(v,u,\mathcal{L}) = \{L \in \mathcal{L} \mid (v,u,L) \in E_{\mathcal{L}}\}$.

Note that in the above formula, each of the sets SL refers to the layers on which two nodes in a redundant pair are linked. Upon this concept, we define the *set of supporting layers sup* for each community C as:

$$sup(C,\mathcal{L}) = \bigcup_{(v,u) \in P_2^C} SL(v,u,\mathcal{L}). \quad (5)$$

Using the above defined $sup(C,\mathcal{L})$, we provide the following definition of *redundancy-based resolution factor*.

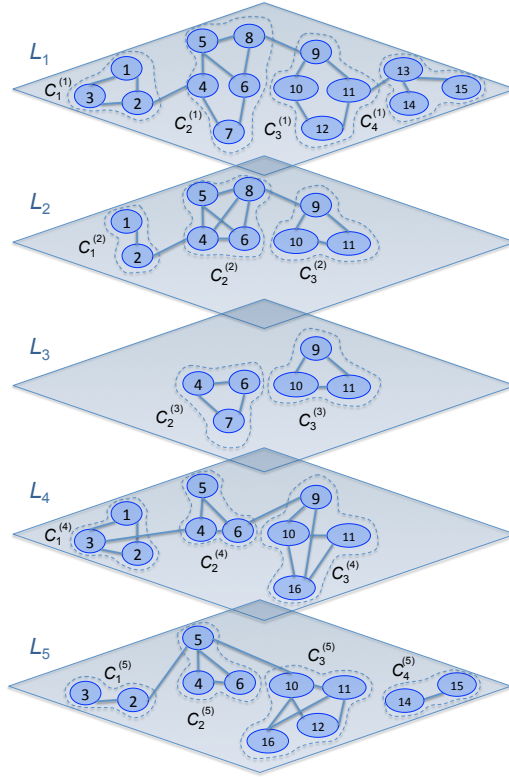


Figure 2: Multilayer network for our running example

Definition 4.2 (Redundancy-based resolution factor). *Given a layer L and a community C , the redundancy-based resolution factor in Eq. (3) is defined as:*

$$\gamma(L, C) = \frac{2}{1 + \log_2(1 + nrp(L, C))} \quad (6)$$

where $nrp(L, C) = |\{s=SL(v, u, \mathcal{L}) \in sup(C, \mathcal{L}) \mid L \in s\}|$ expresses the number of times layer L participates in redundant pairs. \square

Note that $\gamma(L, C)$ ranges in $(0, 1] \cup [2]$. In particular, it ranges in $(0, 1]$ as long as L participates in at least one redundant pair, and it decreases as $nrp(L, C)$ increases; moreover, as special case, $\gamma(L, C)$ is equal to 2 when $nrp(L, C) = 0$.

Example 4.1. *Consider the network with 16 entities and 5 layers shown in Fig. 2, and let us first focus on some specific cases for the computation of the $\gamma(L, C)$ terms. For instance, given community C_4 and layers L_1 and L_5 , the corresponding values of redundancy-based resolution are equal to 2, because L_1, L_5 never participate in redundant pairs for nodes of C_4 . By contrast, layers L_2 and L_5 participate in one redundant pair for community C_1 , which corresponds to*

Table 1: Redundancy-based resolution factor $\gamma(L, C)$ for each community and layer of the example network in Fig. 2.

	L_1	L_2	L_3	L_4	L_5
C_1	0.667	1.000	-	0.667	1.000
C_2	0.525	0.558	0.667	0.667	0.667
C_3	0.602	0.667	0.667	0.602	0.558
C_4	2.000	-	-	-	2.000

the edge linking entities 2 and 3 for L_5 and the edge linking entities 1 and 2 for L_2 ; therefore, the values of redundancy-based resolution associated with C_1 on L_2 and L_5 are equal to 1. Also, the resolution for C_1 on L_1 takes a value lower than 1 since there is more than one redundant pair. Table 1 reports on the entire set of values for the resolution factor computed on the network of Fig. 2.

4.2 Projection-based inter-layer couplings

We propose a general and versatile approach to quantify the strength of coupling of nodes in one layer with nodes on another layer. Our key idea is *to determine the fraction of nodes belonging to a community onto a layer that appears in the projection of the community on another layer, and express the relevance of this projection w.r.t. that pair of layers.*

Given a community $C \in \mathcal{C}$ and layers $L_i, L_j \in \mathcal{L}$, we will use symbols $C^{(i)}$ and $C^{(j)}$ to denote the *projection* of C onto the two layers, i.e., the set of nodes in C that lay on L_i and L_j , respectively. In the following, we define two approaches for measuring inter-layer couplings based on community projection.

For any two layers L_i, L_j and community C , the first approach, we call *symmetric*, determines the relevance of inter-layer coupling of nodes belonging to C as proportional to the fraction of nodes shared between L_i and L_j that belong to C .

Definition 4.3. *Given a community $C \in \mathcal{C}$ and layers $L_i, L_j \in \mathcal{L}$, the symmetric projection-based inter-layer coupling, denoted as $IC_s(C, L_i, L_j)$ and referring to term IC in Eq. (3), is defined as the probability that C lays on L_i and L_j :*

$$IC_s(C, L_i, L_j) = \Pr[C \text{ in } L_i, C \text{ in } L_j] = \frac{|C^{(i)} \cap C^{(j)}|}{|V_i \cap V_j|} \quad (7)$$

□

The above definition assumes that the two events “ C in L_i ” and “ C in L_j ” are independent to each other, and it does not consider that the coupling might have a different meaning depending on the *relevance* a community has on a particular layer in which it is located. By relevance of community we simply mean here the fraction of nodes in a layer graph that belong to the community; therefore, the larger the community in a layer, the more relevant

is w.r.t. that layer. However, we observe that *more relevant community in a layer corresponds to less surprising projection from that layer to another*. This would imply that the inter-layer coupling for that community is less interesting w.r.t. projections of smaller communities, and hence the strength of the coupling might be lowered. We capture the above intuition by the following definition of *asymmetric projection-based inter-layer coupling*.

Definition 4.4. *Given a community $C \in \mathcal{C}$ and layers $L_i, L_j \in \mathcal{L}$, the asymmetric projection-based inter-layer coupling, denoted as $IC_a(C, L_i, L_j)$ and referring to term *IC* in Eq. (3), is defined as the probability that C lays on L_j given that C lays on L_i :*

$$\begin{aligned}
 IC_a(C, L_i, L_j) &= \Pr[C \text{ in } L_j | C \text{ in } L_i] = \\
 &= \frac{\Pr[C \text{ in } L_i, C \text{ in } L_j]}{\Pr[C \text{ in } L_i]} = \\
 &= \frac{|C^{(i)} \cap C^{(j)}|}{|V_i \cap V_j|} \times \frac{|V_i|}{|C^{(i)}|} \tag{8}
 \end{aligned}$$

□

Dealing with layer ordering. Our formulation of multilayer modularity is general enough to account for an available ordering of the layers, according to a given partial order relation.

The previously defined asymmetric inter-layer coupling is well suited to model situations in which we might want to express the inter-layer coupling from a “source” layer to a “destination” layer. Given any two layers L_i, L_j , it may be the case that only comparison of L_i to L_j , or vice versa, is allowed. This is clearly motivated when there exist layer-coupling constraints, thus only some of the layer couplings should be considered in the computation of Q .

In practical cases, we might assume that the layers can be naturally ordered to reflect a predetermined lexicographic order, which might be set, for instance, according to a progressive enumeration of layers or to a chronological order of the time-steps corresponding to the layers. That said, we can consider two special cases of *layer ordering*:

- *Adjacent layer coupling:* $L_i \prec_{\mathcal{L}} L_j$ iff $j = i + 1$ according to a predetermined natural order.
- *Succeeding-layer coupling:* $L_i \prec_{\mathcal{L}} L_j$ iff $j > i$ according to a predetermined natural order.

Note that the adjacent layer coupling scheme requires $\ell - 1$ pairs to consider, while the succeeding-layer coupling scheme involves the comparison between a layer and its subsequent ones, i.e., $(\ell^2 - \ell)/2$ pairs.

Moreover, it should be noted that the availability of a layer ordering enables two variants of the asymmetric projection-based inter-coupling given in Eq. (8). For any two layers $L_i, L_j \in \mathcal{L}$, such that $L_i \prec_{\mathcal{L}} L_j$ holds, we refer to as *inner*

the direct evaluation of $IC_a(C, L_i, L_j)$, and as **outer** the case in which L_i and L_j are switched, i.e., $IC_a(C, L_j, L_i)$.

In the inner case, the strength of coupling is higher as the projection of C on the source layer (i.e., the preceding one in the order) is less relevant; vice versa, the outer case weights more the coupling as the projection on the destination layer (i.e., the subsequent one in the order) is less relevant.

Example 4.2. Consider again the example network of Fig. 2. The asymmetric coupling for the projection of community C_2 from L_2 to L_3 is $IC_a(C_2, L_2, L_3) = (2/5) \times (9/4) = 9/10 = 0.9$ in the inner case, and $IC_a(C_2, L_3, L_2) = (2/5) \times (6/3) = 4/5 = 0.8$ in the outer case.

We hereinafter use symbols IC_{ia} and IC_{oa} to distinguish between the inner asymmetric and the outer asymmetric evaluation cases.

Time-evolving multilayer networks. So far we have assumed that when comparing any two layers L_i, L_j , with $L_i \prec_{\mathcal{L}} L_j$, it does not matter the number of layers between L_i and L_j . Intuitively, we might want to penalize the strength of the coupling as more “distant” L_j is from L_i . This is often the case in time-sliced networks, whereby we want to understand how community structures evolve over time.

In light of the above remarks, we define a refinement of the asymmetric projection-based inter-layer coupling, by introducing a multiplicative factor that smoothly decreases the value of the IC_a function as the temporal distance between L_i and L_j increases.

Definition 4.5. Given a community $C \in \mathcal{C}$ and layers $L_i, L_j \in \mathcal{L}$, such that $L_i \prec_{\mathcal{L}} L_j$, the time-aware asymmetric projection-based inter-layer coupling, denoted as $IC_a^t(C, L_i, L_j)$, is defined as

$$IC_a^t(C, L_i, L_j) = IC_a(C, L_i, L_j) \times \frac{2}{1 + \log_2(1 + j - i)} \quad (9)$$

□

Note that the second term in the above equation is 1 for the adjacent layer coupling scheme, thus making no penalization effect when only consecutive layers are considered.

Example 4.3. Referring again to the example in Fig. 2, in Table 2 we summarize the mean and standard deviation values for the different variants of the inter-layer coupling factor. One remark is that the values for communities C_2 and C_3 are higher than those corresponding to communities C_1 and C_4 . This is mainly due to the representativity of C_2 and C_3 in all layers. The lowest values are obtained for community C_4 , which is in fact less represented than other communities (only in layers L_1 and L_5). For instance, let us focus on this community. The mean inter-layer coupling factor IC_{oa}^{Suc} for community C_4 is 0.11, since: $|C_4^{(5)} \cap C_4^{(1)}| = 2$, $|V_5 \cap V_1| = 10$ (which is exactly the size of L_5 without

Table 2: Different variants of the inter-layer coupling factor, for each community of the example network in Fig. 2. Values are cumulated over the admissible pairings of layers. Mean and standard deviation values are reported.

	IC_s	$IC_{ia} \equiv IC_{oa}$	IC_{ia}^{Adj}	IC_{oa}^{Adj}	IC_{ia}^{Suc}	IC_{oa}^{Suc}
C_1	0.135 ± 0.038	0.612 ± 0.214	0.444 ± 0.314	0.525 ± 0.071	0.619 ± 0.274	0.606 ± 0.159
C_2	0.398 ± 0.096	1.105 ± 0.284	1.115 ± 0.157	1.192 ± 0.320	1.018 ± 0.245	1.193 ± 0.305
C_3	0.416 ± 0.074	1.148 ± 0.258	1.188 ± 0.239	1.088 ± 0.118	1.249 ± 0.306	1.048 ± 0.158
C_4	0.018 ± 0.000	0.091 ± 0.000	0.000 ± 0.000	0.000 ± 0.000	0.091 ± 0.000	0.110 ± 0.000

Table 3: Multilayer modularity for the various combinations of resolution and inter-layer coupling terms, on the example network in Fig. 2. Community-specific values correspond to the modularity contribution given by each particular community to the overall modularity.

	γ, IC_s	γ, IC_{ia}	γ, IC_{oa}	γ, IC_{ia}^{Adj}	γ, IC_{oa}^{Adj}	γ, IC_{ia}^{Suc}	γ, IC_{oa}^{Suc}	$\gamma, IC=0$	$\gamma=1, IC_s$	$\gamma=1, IC_{ia}$	$\gamma=1, IC_{oa}$	$\gamma=1, IC=0$
C_1	0.064	0.098	0.098	0.129	0.131	0.142	0.141	0.126	0.063	0.097	0.097	0.123
C_2	0.164	0.214	0.214	0.318	0.320	0.317	0.329	0.310	0.162	0.213	0.213	0.307
C_3	0.161	0.213	0.213	0.313	0.309	0.325	0.312	0.266	0.160	0.212	0.212	0.299
C_4	0.022	0.028	0.028	0.044	0.044	0.045	0.045	0.048	0.022	0.027	0.027	0.047
Q	0.411	0.554	0.554	0.803	0.804	0.828	0.827	0.750	0.408	0.550	0.550	0.777

node 16), $|V_5|=11$ and $|C_4^{(5)}|=2$; this determines an inter-layer coupling factor of 1.1, which is divided by the admissible pairings of layers, i.e., 10. On the contrary, the mean IC_{oa}^{Adj} for C_4 is equal to zero, because the projection of this community is always empty when the adjacent coupling scheme is used.

Finally, Table 3 reports the multilayer modularity values, including the community-specific contributions. Note that, regardless of the settings of γ and IC factors, communities C_2 and C_3 obtain the highest values of modularity, which is mainly determined since they are disconnected from the rest of the graph at layer L_3 . In general, it should be noted that the contribution given by each community is consistent w.r.t. the various settings of γ and IC factors. Also, it is interesting to note that discarding the inter-layer couplings ($IC=0$, which corresponds to the 9th and 13th columns) can lead to values of community-modularity and global modularity that tend to be much higher than the corresponding cases with $IC \neq 0$. This overestimation can also occur, though to a lesser extent, when fixing $\gamma=1$ (13th column) vs. redundancy-based γ (9th column). Also, it is worth noting that using the redundancy-based resolution factor γ with unordered layers (2nd, 3rd and 4th columns) increases the community as well as global modularity vs. the same cases with $\gamma=1$ (10th, 11th, and 12th columns).

4.2.1 Relations between the resolution and inter-layer coupling factors

Both factors take into consideration the network context, however they differ in that $\gamma(L, C)$ considers a ‘‘global’’ multiplex context, whereas IC considers a ‘‘local’’ multiplex context. Intuitively, $\gamma(L, C)$ is defined for each valid layer-community pair according to the status of the links among nodes in community C that lays on L versus their status on the other layers. By contrast, IC con-

siders the status of the same community from one layer to another comparable layer.

In terms of numerical comparison, when the size of the community structure tends to the number of nodes of the network, $\gamma(L, C)$ tends to increase (i.e., to the maximum value of 2) while IC tends to decrease (i.e., to zero).

4.3 Properties of the proposed multilayer modularity

We provide theoretical insights on Q , focusing on the effect of increase in the size of the community structure and on the analytical derivation of the range of values of Q .

4.3.1 Effect of increase in the number of communities

We discuss the effect of increasing k (i.e., decreasing the average size of communities in \mathcal{C}) by distinguishing three configurations of Q : (i) symmetric inter-layer coupling, (ii) asymmetric inter-layer coupling, and (iii) ordered layers.

In the first case, Q tends to have a monotonic decreasing trend. This is easily explained by the combination of three contingencies. The first one is an average decrease in the internal degree d_L^{int} . The second contingency is an increase in the redundancy-based resolution factor γ : in fact, smaller communities correspond to lower probability of observing redundant pairs within communities over different layers; this decreases the logarithmic term in the resolution factor, which will progressively tend to 2 (maximum value). The third contingency is a decrease in the inter-layer coupling factor IC_s , since the size of community intersection becomes increasingly smaller as the community size decreases.

By contrast, when equipped with the asymmetric projection-based inter-layer coupling IC_a , Q tends to differ from a monotonic decreasing trend because of the bias term $\frac{|V_i|}{|C^{(i)}|}$, which increases with communities of smaller size.

In the third case (i.e., ordered layers), Q can again follow an increasing or decreasing trend. Recall that the term $d(V_{\mathcal{L}})$ includes the contribution of the inter-layer edges, which obviously are fewer when the layer couplings are order-dependent. A decrease in the number of inter-layer couplings also makes the decrease in the actual connectivity term (i.e., $\frac{d_j^{int}(C)}{d(V_{\mathcal{L}})}$) slower as k increases, since $d(V_{\mathcal{L}})$ is smaller than in the unordered-layer contingency. Consequently, the inter-layer coupling term could compensate the actual connectivity term, which will result in increasing the value of Q . Finally, considering time-aware asymmetric inter-layer coupling, Q is more likely to follow a decreasing trend because of the effect due to the smoothing term $\frac{2}{1+\log_2(1+j-i)}$, which penalizes IC_a for any two no time-consecutive layers. Consequently, since the inter-layer coupling factor IC_a^t is smaller than IC_a , Q could monotonically decrease despite the bias term $\frac{|V_i|}{|C^{(i)}|}$ in IC_a^t .

4.3.2 Lower and upper bounds

To determine the range of values of the basic modularity in simple graphs, the theoretical frameworks previously studied in [4] and [24] define two canonical structures to support the analytical computation of the minimum and maximum value of the modularity, respectively. More specifically, the former work proved that any *bipartite* graph with the canonical *two-way clustering* obtains the minimum value of modularity, whereas the latter work proved that the maximum modularity is reached in a graph composed of disjoint cliques.

Following the lead of the above works, here we provide theoretical results about the analytical derivation of the lower bound and upper bound of our proposed multilayer modularity.

Proposition 1. *Given a multilayer network $G_{\mathcal{L}} = (V_{\mathcal{L}}, E_{\mathcal{L}}, \mathcal{V}, \mathcal{L})$, with $n = |\mathcal{V}|, \ell = |\mathcal{L}|$, and a community structure \mathcal{C} for $G_{\mathcal{L}}$, the lower bound of Q is as follows:*

$$Q(\mathcal{C}) = -\frac{n^2\ell}{(n\ell + 2p)^2} + \frac{4(1 + \eta)p}{n^2(n\ell + 2p)}, \quad (10)$$

with $\eta = 0$ for IC_s and $\eta = 1$ for IC_a , and $p = \sum_{L \in \mathcal{L}} |\mathcal{P}(L)|$ is the total number of valid layer-pairings.

Proof. Proof is reported in the **Appendix**.

Proposition 2. *Given a multilayer network $G_{\mathcal{L}} = (V_{\mathcal{L}}, E_{\mathcal{L}}, \mathcal{V}, \mathcal{L})$, with $n = |\mathcal{V}|, \ell = |\mathcal{L}|$, and a community structure \mathcal{C} for $G_{\mathcal{L}}$, the upper bound of Q is as follows:*

$$Q(\mathcal{C}) = 2 \left[\frac{1}{2} \frac{\left(\frac{n}{2} - 1\right)\ell}{\left(\frac{n}{2} - 1\right)\ell + p} - \gamma\ell \left(\frac{1}{2} \frac{\left(\frac{n}{2} - 1\right)}{\left(\frac{n}{2} - 1\right)\ell + p} \right)^2 + \frac{(1 + \eta)p}{n^2\left(\frac{n}{2} - 1\right)\ell + n^2p} \right] \quad (11)$$

with $\eta = 0$ for IC_s and $\eta = 1$ for IC_a , and $p = \sum_{L \in \mathcal{L}} |\mathcal{P}(L)|$ is the total number of valid layer-pairings.

Proof. Proof is reported in the **Appendix**.

Note that, in the special case for $\beta = 0$, i.e., the inter-layer coupling factor is discarded, the lower bound of Q is

$$Q(\mathcal{C}) = -\frac{1}{\ell}. \quad (12)$$

Analogously, the upper bound of Q is rewritten as:

$$Q(\mathcal{C}) = \frac{2\ell - \gamma}{2\ell}, \quad (13)$$

with $\gamma = 2(1 + \log_2(1 + \frac{n}{2}(\frac{n}{2} - 1)))^{-1}$.

5 Evaluation Methodology

We discuss here the evaluation networks (Sect. 5.1), the multilayer community detection methods (Sect. 5.2), and the experimental settings (Sect. 5.3).

5.1 Datasets

Our selection of network datasets was motivated to fulfill the *reproducibility* requirement: in fact, all of our evaluation datasets, including both real-world networks and synthetic generators, are publicly available. Moreover, we also took the opportunity of diversifying the choice of real-world networks by considering various domains that are profitably modeled as multilayer networks.

5.1.1 Real-world network datasets

We considered 10 real-world multilayer network datasets. *AUCS* [42, 43] describes relationships among university employees: work together, lunch together, off-line friendship, friendship on Facebook, and coauthorship. EU-Air transport network [42] (*EU-Air*, for short) represents European airport connections considering different airlines. FAO Trade network (*FAO-Trade*) [44] represents different types of trade relationships among countries, obtained from FAO (Food and Agriculture Organization of the United Nations). *FF-TW-YT* (stands for FriendFeed, Twitter, and YouTube) [12] was built by exploiting the feature of FriendFeed as social media aggregator to align registered users who were also members of Twitter and YouTube. Flickr refers to the dataset studied in [45]. We used the corresponding timestamped interaction network whose links express “who puts a favorite-marking to a photo of whom”. We extracted the layers on a month-basis and aggregated every six (or more) months. *GH-SO-TW* (stands for GitHub, StackOverflow and Twitter) [46] is another cross-platform network where edges express followships on Twitter and GitHub, and “who answers to whom” relations on StackOverflow. *Higgs-Twitter* [42] represents friendship, reply, mention, and retweet relations among Twitter users. London transport network [18] (*London*, for short) models three types of connections of train stations in London: underground lines, overground, and DLR. ObamaInIsrael2013 [47] (*Obama*, for short) models retweet, mention, and reply relations of users of Twitter during Obama’s visit to Israel in 2013. 7thGraders [18] (*VC-Graders*, for short) represents students involved in friendship, work together, and affinity relations in the class. Table 4 reports for each dataset, the size of set \mathcal{V} , the number of edges in all layers, and the average coverage of node set (i.e., $1/|\mathcal{L}|\sum_{L_i \in \mathcal{L}}(|V_i|/|\mathcal{V}|)$). The table also shows basic, monoplex structural statistics (degree, average path length, and clustering coefficient) for the layer graphs of each dataset.

5.1.2 Synthetic network datasets

Besides the real-world network data, we generated four synthetic multilayer network datasets. Our goal was the evaluation of the multilayer modularity Q

Table 4: Main characteristics of our evaluation network datasets. Mean and standard deviation over the layers are reported for degree, average path length, and clustering coefficient statistics.

	#entities ($ \mathcal{V} $)	#edges	#layers (ℓ)	node set coverage	degree	avg. path length	clustering coefficient
<i>AUCS</i>	61	620	5	0.73	10.43 ± 4.91	2.43 ± 0.73	0.43 ± 0.097
<i>EU-Air</i>	417	3 588	37	0.13	6.26 ± 2.90	2.25 ± 0.34	0.07 ± 0.08
<i>FAO-Trade</i>	214	318 346	364	1.00	7.35 ± 6.17	2.43 ± 0.39	0.31 ± 0.11
<i>FF-TW-YT</i>	6 407	74 836	3	0.58	9.97 ± 7.27	4.18 ± 1.27	0.13 ± 0.09
<i>Flickr</i>	789 019	17 071 325	5	0.33	23.15 ± 5.61	4.50 ± 0.60	0.04 ± 0.01
<i>GH-SO-TW</i>	55 140	2 944 592	3	0.68	41.29 ± 45.09	3.66 ± 0.62	0.02 ± 0.01
<i>Higgs-Twitter</i>	456 631	16 070 185	4	0.67	18.28 ± 31.20	9.94 ± 9.30	0.003 ± 0.004
<i>London</i>	369	441	3	0.36	2.12 ± 0.16	11.89 ± 3.18	0.036 ± 0.032
<i>Obama</i>	2 281 259	4 061 960	3	0.50	4.27 ± 1.08	13.22 ± 4.49	0.001 ± 0.0005
<i>VC-Graders</i>	29	518	3	1.00	17.01 ± 6.85	1.66 ± 0.22	0.61 ± 0.89

on different network models. Two out of the four networks are composed of 2 layers and 256 entities. In one network, hereinafter referred to as *ER-ER*, the two layers are Erdős-Rényi (ER) random graphs. In the second network, dubbed *LFR-ER*, the first layer is generated by the Lancichinetti-Fortunato-Radicchi (LFR) benchmark, while the second layer is an Erdős-Rényi random graph. The other two networks are composed of 4 layers and 128 nodes. Both networks are characterized by two Erdős-Rényi layers and two layers built as Girvan-Newman (GN) graphs, but they differ in the layer ordering: *GN-ER-GN-ER* in the first network, and *GN-ER-ER-GN* in the second network.

Moreover, mainly for purposes of efficiency evaluation, we generated a set of synthetic multilayer networks using the Lancichinetti-Fortunato-Radicchi (LFR) benchmark. In particular, single-layer network datasets were provided by the LFR benchmark using a variable number of nodes with steps of 128 until 1024. Also, the maximum and average node degrees were set to 16, and the mixing coefficient μ was set to 0.1. Each network dataset was characterized by four communities. From each of such networks, a multilayer network was created by replicating the LFR single-layer from 2 to 10.

5.2 Community detection methods

We resorted to state-of-the-art methods for community detection in multilayer networks, which belong to the two major approaches, namely *aggregation* and *direct* methods. The former detect a community structure separately for each network layer, after that an aggregation mechanism is used to obtain the final community structure, while the latter directly work on the multilayer graph by optimizing a multilayer quality-assessment criterion. (Note that while it is possible to flatten the multilayer graph in order to apply on it any conventional community detection algorithm, this approach can be too simplistic, since, e.g., it would not permit to investigate about the temporal evolution of communities.)

As exemplary methods of the aggregation approach, we used *Principal Modularity Maximization* (PMM) [48] and *Enhanced Modularity-driven Ensemble-based Multilayer Community Detection* (M-EMCD*) [20]. PMM aims to find a

concise representation of features from the various layers (dimensions) through structural feature extraction and cross-dimension integration. Features from each dimension are first extracted via modularity maximization, then concatenated and subjected to PCA to select the top eigenvectors, which represent possible community partitions. Using these eigenvectors, a low-dimensional embedding is computed to capture the principal patterns across all the dimensions of the network, finally a k -means on this embedding is carried out to discover a community structure. M-EMCD* is a parameter-free extension of the M-EMCD method proposed in [19]. Given an ensemble of community structures available for a multilayer network, M-EMCD optimizes a consensus objective function to discover a consensus solution with maximum modularity, subject to the constraint of being searched over a hypothetical space of consensus community structures that are valid w.r.t. the input ensemble and topologically bounded by two baseline solutions. To detect the initial cluster memberships of nodes, M-EMCD utilizes a consensus or co-association matrix, which stores the fraction of clusterings in which any two nodes are assigned to the same cluster. To filter out noisy, irrelevant co-association, a user-specified threshold must be specified. Besides introducing flexibility in community assignments of nodes during the modularity optimization, M-EMCD* overcomes the limitation of setting such a parameter of minimum co-association, by providing a parameter-free identification of consensus clusters based on generative models for graph pruning.

As for the direct methods, we resorted to *Generalized Louvain* (GL) [15] and *Locally Adaptive Random Transitions* (LART) [17]. GL extends the classic Louvain method using multislice modularity, so that each node-layer tuple is assigned separately to a community. Majority voting is adopted to decide the final assignment of an entity node to the community that contains the majority of its layer-specific instances. LART is a random-walk based method. It first runs a different random walk for each layer, then a dissimilarity measure between nodes is obtained leveraging the per-layer transition probabilities. A hierarchical clustering method is used to produce a hierarchy of communities which is eventually cut at the level corresponding to the best value of multislice modularity.

It should be emphasized that we selected the above methods because, while having different characteristics, they all use modularity either as optimization criterion (GL, PMM and M-EMCD*) or as evaluation criterion to produce the final community structure (LART).

Note also that PMM requires the desired number of communities (k) as input. Due to different size of our evaluation datasets, we devised several configurations of variation of parameter k in PMM, by reasonably adapting each of the configuration range and increment step to the network size. Concerning M-EMCD*, we used the *marginal likelihood filter* (MLF) to perform parameter-free detection of the number of communities [20].

It should be noted that the selected methods actually discover different community structures, thus supporting our choice in terms of diversity of evaluation scenarios for the two competing modularity measures under study. Table 5 re-

Table 5: Number of communities found by GL, LART, PMM and M-EMCD* with MLF model-filter on the real-world network datasets

	GL	LART	PMM	M-EMCD*
<i>AUCS</i>	5	27	2	13
<i>EU-Air</i>	10	381	5	39
<i>FAO-Trade</i>	12	-	10	11
<i>FF-TW-YT</i>	749	-	10	115
<i>GH-SO-TW</i>	87	-	10	392
<i>Flickr</i>	12290	-	10	7660
<i>Higgs-Twitter</i>	15218	-	10	121
<i>London</i>	21	339	30	46
<i>Obama</i>	297062	-	10	328367
<i>VC-Graders</i>	3	6	2	16

ports the number of communities of the solutions found by the various methods on the real-world network datasets. (The number of communities k in PMM is selected according to the solution with highest modularity value.) We found that GL tends to discover a high number of communities for larger networks (i.e., *Flickr*, *Higgs-Twitter*, *FF-TW-YT*, and *Obama*), and the size distribution of these communities (results not shown) is highly right-skewed on the larger networks, while it is moderately left-skewed on the remaining datasets. A similar result can be observed in M-EMCD* for the different networks, although in *Higgs-Twitter* and *FF-TW-YT* (resp. *GH-SO-TW*) the number of communities is much lower (resp. higher) than in GL. By contrast, the best performances of PMM usually correspond to a low and quite stable number of communities. Also, LART generally tends to produce much more communities than the other methods, on the networks for which it is able to discover communities.

As a final general remark, we used the original implementations of the selected methods, based on the source code made available by the respective authors. We emphasize that it is beyond the goals of this work to make any performance improvement in the community detection methods under study, which hence are considered here with no intent of comparative evaluation and with all their limitations. (This justifies, in particular, the inability of LART in terminating the task for some network datasets.)

5.3 Experimental settings

We carried out GL, PMM, LART and M-EMCD* methods on each of the network datasets and measured, for each community structure solution, our proposed multilayer modularity (Q) as well as the Mucha et al.’s multislice modularity (Q_{ms}).

We evaluated Q using the redundancy-based resolution factor $\gamma(L, C)$ with either the symmetric (IC_s) or the asymmetric (IC_a) projection-based inter-layer coupling. We also considered cases corresponding to ordered layers, using either the adjacent-layer scheme or the succeeding-layer scheme, and for both schemes

Table 6: Multilayer modularity Q and multislice modularity Q_{ms} on GL community structures of the four synthetic networks.

	#comm. by GL	Q_{ms}	$\gamma = 1,$ IC_s	$\gamma = 1,$ $IC_{ia} \equiv IC_{oa}$	$\gamma,$ $\beta = 0$	$\gamma,$ IC_s	$\gamma,$ $IC_{ia} \equiv IC_{oa}$
ER-ER	10	0.249	0.192	0.196	0.290	0.258	0.262
LFR-ER	16	0.486	0.404	0.411	0.486	0.434	0.441
GN-ER-GN-ER	4	0.429	0.432	0.436	0.552	0.471	0.475
GN-ER-ER-GN	4	0.429	0.432	0.436	0.552	0.471	0.475

considering inner (IC_{ia}) as well as outer (IC_{oa}) asymmetric coupling. We further evaluated the case of temporal ordering, using the time-aware asymmetric projection-based inter-layer coupling. Yet, we considered the particular setting of uniform resolution (i.e., $\gamma(L, C) = 1$, for each layer L and community C).

As for Q_{ms} , we devised two settings: the first by varying ω within $[0..2]$ while fixing $\gamma = 1$, the second by varying γ and $\omega = 1 - \gamma$ [15].

6 Results

We organize our main experimental results into two parts, depending on whether layer ordering was considered in the evaluation networks. Experiments were carried out on an Intel Core i7-3960X CPU @3.30GHz, 64GB RAM machine.

6.1 Evaluation with unordered layers

6.1.1 Synthetic network datasets

Table 6 reports the multilayer modularity Q , multislice modularity Q_{ms} and number of communities obtained by the GL solution on the four synthetic networks.

One first remark is that using the redundancy-based resolution factor γ always leads to higher Q w.r.t. the cases corresponding to γ fixed to 1. In particular, we observe gains up to 0.1 on ER-ER, 0.07 on LFR-ER, and 0.12 on GN-ER-GN-ER and GN-ER-ER-GN.

Another remark is that the fully combination of resolution and inter-layer coupling factors (i.e., rightmost two columns) tends to lower the value of Q w.r.t. the cases corresponding to varying γ with $\beta = 0$ (i.e., third last column); moreover, the asymmetric inter-layer coupling results in a higher Q w.r.t. the symmetric setting of IC . This would hint that when the normalization term in the Q equation accounts for the inter-layer couplings, this results in lowering the value of Q , which is turn smoother when the asymmetric setting is used.

Comparing Q and Q_{ms} , it should be noted that the two measures behave consistently on ER-ER vs. LFR-ER, i.e., the presence of a layer with a (LFR) modular structure actually leads to an increase in both modularity measures w.r.t. ER-ER. By contrast, Q tends increase faster than Q_{ms} on the two GN-ER networks: this can be explained since a higher number of layers (as occurs

Table 7: Multilayer modularity Q on GL community structures

	$\gamma(L, C)$		$\gamma = 1$	
	IC_a	IC_s	IC_a	IC_s
<i>AUCS</i>	0.41	0.37	0.39	0.35
<i>EU-Air</i>	0.04	0.03	0.04	0.03
<i>FAO-Trade</i>	0.11	0.03	0.11	0.03
<i>FF-TW-YT</i>	0.50	0.42	0.42	0.34
<i>Flickr</i>	0.32	0.31	0.28	0.27
<i>GH-SO-TW</i>	0.40	0.40	0.35	0.35
<i>Higgs-Twitter</i>	0.15	0.13	0.14	0.12
<i>London</i>	0.35	0.26	0.34	0.26
<i>Obama</i>	0.43	0.32	0.43	0.32
<i>VC-Graders</i>	0.54	0.53	0.44	0.43

for the two GN-ER networks than for the ER-ER and LFR-ER networks) has a higher effect on the inter-layer coupling factor IC , which is not present in Q_{ms} .

6.1.2 Real-world network datasets

Tables 7–9 and Fig. 3 report Q measurements on the community structure solutions obtained by the various community detection methods.

Concerning GL (Table 7), we observe that with the exception of *GH-SO-TW* on which effects on Q are equivalent, using IC_a leads to higher Q than IC_s . On average over all networks, using IC_a yields an increment of 13.4% and 14.6% (with γ fixed to 1) w.r.t. the value of Q corresponding to IC_s . This higher performance of Q due to IC_a supports our initial hypothesis on the opportunity of asymmetric inter-layer coupling. It is also interesting to note that, when fixing γ to 1, Q decreases w.r.t. the setting with redundancy-based resolution $\gamma(L, C)$ — decrement of 11% and 12% using IC_a and IC_s , respectively.

Table 8 shows results obtained from LART solutions. (Due to memory-resource and efficiency issues shown by the currently available implementation of LART, we are able to report results only on some networks). We observe that the relative performance difference between IC_s and IC_a settings is consistent with results found in the GL evaluation; this difference is even extreme (0.98 or 0.99) on *EU-Air* and *London*, which is likely due also to the different sizes of community structures detected by the two methods (cf. Sect. 5.2).

Table 9 shows results obtained by M-EMCD* solutions. Also in this case, using IC_a generally leads to better Q than IC_s , regardless of the setting of γ . In particular, the observed increase is higher in *VC-Graders* and *London* (0.2), followed by *AUCS* (0.18) and *Obama* (0.13). Moreover, when fixing γ to 1, in most cases Q decreases (0.01-0.06) w.r.t. the setting with redundancy-based resolution $\gamma(L, C)$.

Figure 3 shows how Q varies in function of the number (k) of clusters given as input to PMM. One major remark is that Q tends to decrease as k increases. This holds consistently for the configuration of Q with symmetric inter-layer

Table 8: Multilayer modularity Q on LART community structures

	$\gamma(L, C)$		$\gamma = 1$	
	IC_a	IC_s	IC_a	IC_s
<i>AUCS</i>	0.47	0.19	0.43	0.15
<i>EU-Air</i>	1.00	0.02	1.00	0.02
<i>London</i>	1.00	0.01	1.00	0.01
<i>VC-Graders</i>	0.30	0.28	0.22	0.20

Table 9: Multilayer modularity Q on M-EMCD* community structures

	$\gamma(L, C)$		$\gamma = 1$	
	IC_a	IC_s	IC_a	IC_s
<i>AUCS</i>	0.51	0.33	0.50	0.32
<i>EU-Air</i>	0.20	0.14	0.20	0.14
<i>FAO-Trade</i>	0.02	0.03	0.02	0.03
<i>FF-TW-YT</i>	0.47	0.41	0.47	0.41
<i>Flickr</i>	0.37	0.35	0.31	0.29
<i>GH-SO-TW</i>	0.64	0.63	0.61	0.60
<i>Higgs-Twitter</i>	0.58	0.58	0.52	0.52
<i>London</i>	0.46	0.26	0.46	0.25
<i>Obama</i>	0.42	0.29	0.42	0.29
<i>VC-Graders</i>	0.52	0.32	0.50	0.30

coupling; in fact, as discussed in Sect. 4.3.1, the decrease of Q for increasing k depends on a combination of decrease of the internal degree d_L^{int} , decrease of the symmetric inter-layer coupling factor IC_s , and increase of the redundancy-based resolution factor $\gamma(L, C)$. Moreover, values of Q corresponding to IC_a tend to be close to the ones obtained for IC_s on the large networks, while on the smaller ones, IC_a trends are above IC_s , by diverging for high k in some cases; in particular, in *London* modularity for IC_a follows a rapidly, roughly linear increasing trend with k ; even more evident is the divergence of the IC_s and IC_a trends for *AUCS*. Again, as we previously discussed in Sect. 4.3.1, this is due to the bias term $\frac{|V_i|}{|C^{(i)}|}$ of IC_a , which increases with communities of smaller size. Note that, from an inspection of the behavior of Q for higher regimes of k , we also found that Q values eventually tend to stabilize below 1. As concerns the setting with γ fixed to 1 (results not shown), while the trends of Q for IC_a and for IC_s do not change significantly, the values are typically lower than those obtained with redundancy-based resolution, which is again consistent with results observed for GL, LART and M-EMCD* evaluations.

Correlation analysis. We investigated whether any correlation may exist at *community-level* between the value of Q and selected statistics based on structural characteristics of the input network. For this purpose, we focused on the average path length, clustering coefficient, redundancy, and node- and edge-set coverage, for each community in an evaluation network; note that the latter two statistics are computed as, given a community C , the fraction of

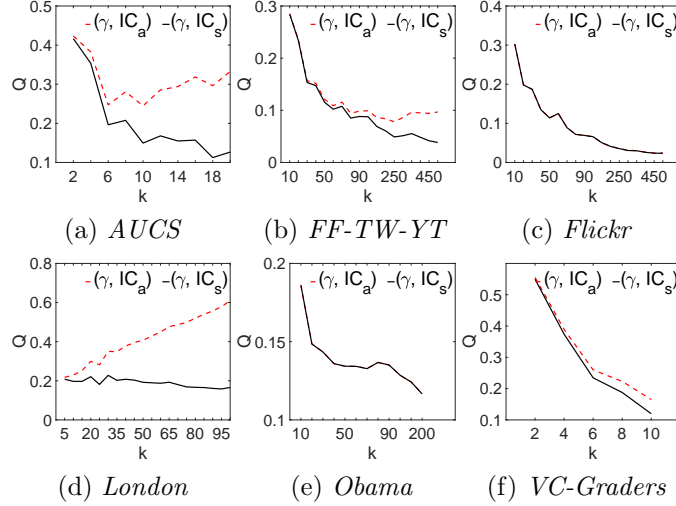


Figure 3: Multilayer modularity Q on PMM community structure solutions

nodes (resp. edges) in a layer L_i that belong to C , averaged over all layers in the network.

Figure 4 shows the correlation between each of the above structural characteristics and the values of Q , with redundancy-based resolution factor $\gamma(L, C)$ and IC_s , on the solution found on selected networks by GL, M-EMCD* and PMM; for the latter, k was chosen as that corresponding to the best modularity performance. Note also that the correlation results obtained by Q with $\gamma = 1$ and IC_s , $\gamma = 1$ and IC_a , $\gamma(L, C)$ only, and combination of $\gamma(L, C)$ and IC_a , do not show significant differences, hence their presentation is discarded. Looking at the three plots in the figure, we observe a mid-high positive correlation of Q with the topological measures in most cases. More in detail, in Fig. 4 (a) the modularity of the solution found by GL on *EU-Air* shows an average correlation of 0.85 with the other measures. Also, an average correlation of 0.95 and 0.96 is obtained between Q and respectively node-set and edge-set coverage on *FF-TW-YT*. For *AUCS*, Q has a positive correlation of 0.76 with clustering coefficient and a negative correlation with the other measures. For *VC-Graders*, Q shows a positive correlation with all measures except with redundancy. For *London* and *GH-SO-TW*, the correlation is up to 0.5. For *FAO-Trade*, Q shows a higher correlation up to 1 with node-set and edge-set coverage, and a lower correlation up to 0.5 with average path length, clustering coefficient and redundancy. Considering Fig. 4 (b), the multilayer modularity Q of the solution found by PMM shows an average correlation of 0.99 with clustering coefficient for *EU-Air*, of 1 and 0.92 with average path length, node-set and edge-set coverage for *AUCS* and *FF-TW-YT*, respectively, and of 1 with redundancy for *VC-Graders*. On the contrary, a correlation of -1 is obtained between Q and the clustering coefficient and redundancy for *AUCS*, and between Q and all

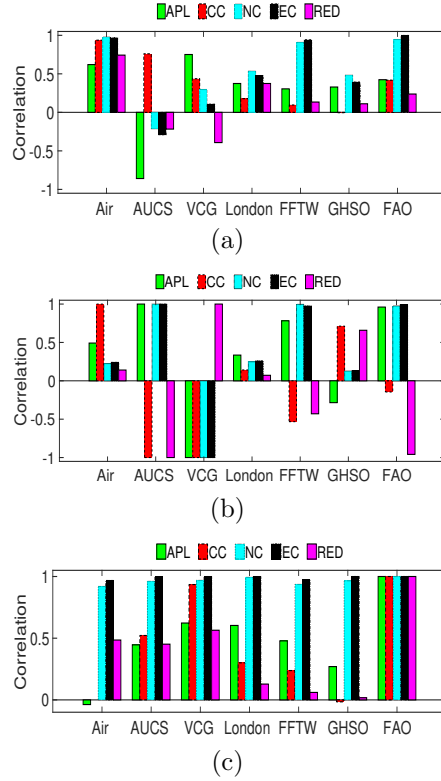


Figure 4: Pearson correlation coefficient between average path length (APL), clustering coefficient (CC), node-set coverage (NC), edge-set coverage (EC), and redundancy (RED) and the multilayer modularity Q with $\gamma(L, C)$ and IC_s computed on the solution found by (a) GL, (b) PMM, and (c) M-EMCD* for selected networks. Each statistic is computed at community-level

measures except the redundancy for *VC-Graders*. For *FAO-Trade*, Q shows a positive correlation up to 1 with average path length, node-set and edge-set coverage, and a negative correlation up to -1 with the redundancy. A weakly negative correlation is shown between Q and clustering coefficient. In the other cases, the correlation ranges between -0.5 and 0.5. Finally, considering Fig. 4 (c), the multilayer modularity Q of the solution found by M-EMCD* shows a very high correlation with node-set and edge-set coverage in all networks. Also, Q shows a correlation with the average path length which is up to 0.5 in all networks, with the only exception of *EU-Air* and *GH-SO-TW*. For redundancy and clustering coefficient, Q obtains a high correlation with clustering coefficient and redundancy in *FAO-Trade* and with clustering coefficient in *VC-Graders*.

Figure 5 shows the correlation between various settings of Q and the previously analyzed set of statistics for solutions obtained by LART. Looking at the

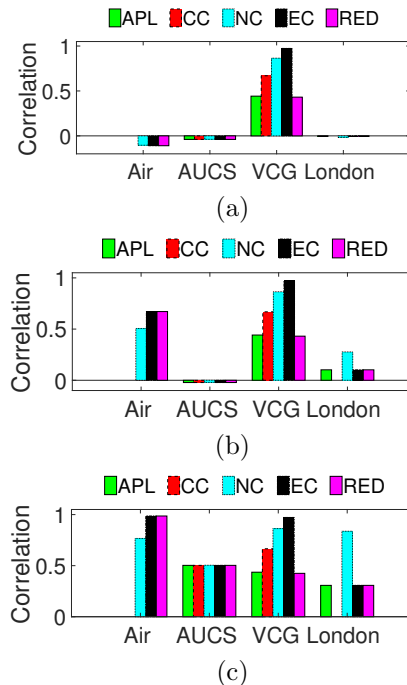


Figure 5: Pearson correlation coefficient between average path length (APL), clustering coefficient (CC), node-set coverage (NC), edge-set coverage (EC), and redundancy (RED) and the multilayer modularity Q with: (a) $\gamma(L, C)$, (b) $\gamma(L, C)$ and IC_s , and (c) $\gamma(L, C)$ and IC_a computed on the solution found by LART for the different real-world network datasets. Each statistics is computed at community-level

plots, Q obtains the highest correlation with the edge-set coverage, followed by the node-set coverage, clustering coefficient and redundancy. Overall, results by LART confirm the trends observed for GL and PMM, with even higher tendency to positive correlation in general. Remarkably, this particularly holds when Q involves the inter-layer coupling terms, with IC_a leading to higher correlation than IC_s .

6.2 Evaluation with ordered layers

In this section we focus on evaluation scenarios that correspond to the specification of an ordering of the set of layers. We will present results on the real-world networks *EU-Air* and *Flickr*. The former was chosen because of its highest dimensionality (i.e., number of layers) over all datasets, the latter is a time-evolving multilayer network and was chosen for evaluating the time-aware asymmetric inter-layer coupling.

Table 10 summarizes results by GL, LART and M-EMCD* on *EU-Air*, corre-

Table 10: Multilayer modularity Q , with layer ordering, from GL, LART and M-EMCD* community structures, on *EU-Air*

	$\gamma(L, C)$				$\gamma = 1$			
	IC_{ia}^{Suc}	IC_{oa}^{Suc}	IC_{ia}^{Adj}	IC_{oa}^{Adj}	IC_{ia}^{Suc}	IC_{oa}^{Suc}	IC_{ia}^{Adj}	IC_{oa}^{Adj}
GL	0.786	0.734	0.512	0.511	0.783	0.729	0.504	0.503
LART	0.981	0.972	0.665	0.656	0.981	0.972	0.664	0.656
M-EMCD*	0.997	0.998	0.970	0.969	0.997	0.999	0.974	0.973

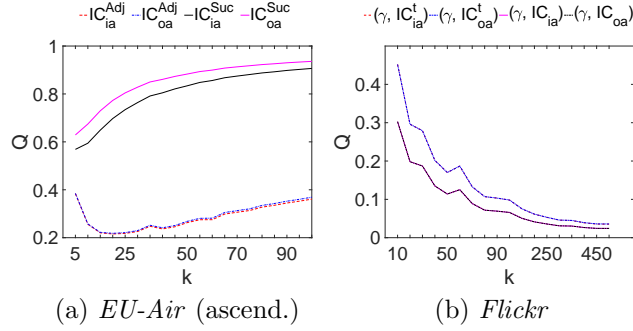


Figure 6: Multilayer modularity Q of PMM solutions with layer ordering.

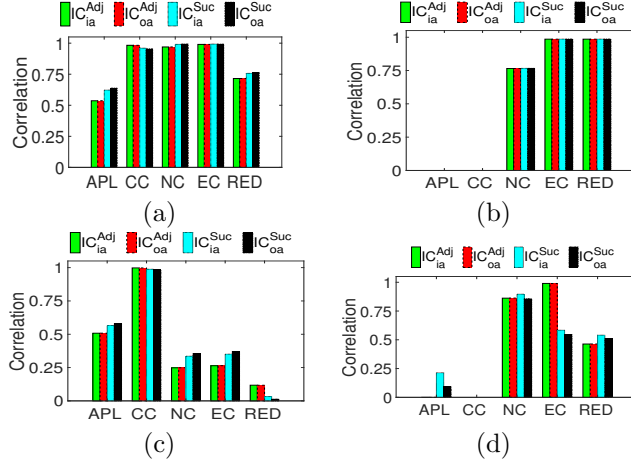


Figure 7: Pearson correlation coefficient between average path length (APL), clustering coefficient (CC), node coverage (NC), edge coverage (EC), redundancy (RED), and the multilayer modularity Q with $\gamma(L, C)$ and IC_{ia}^{Adj} , IC_{oa}^{Adj} , IC_{ia}^{Suc} , IC_{oa}^{Suc} , and ascendent layer ordering, computed on the solution found by (a) GL, (b) LART, (c) PMM, and (d) M-EMCD* on the *EU-Air* network. Each statistics is computed at community-level

sponding to adjacent and succeeding-layer coupling. We observe that, regardless of the setting of the resolution factor, values of Q with succeeding-layer coupling

are higher than the corresponding ones for the adjacent layer coupling scheme. This suggests that the impact on the inter-layer coupling term is higher when all ordered pairs of layers are taken into account, than when only adjacent pairs are considered. In this regard, recall that the total degree of the multilayer graph, which normalizes the inter-layer coupling term as well, is properly computed according to the actual number of inter-layer couplings considered, depending on whether adjacent or succeeding-layer scheme was selected.

The above result is also confirmed by PMM, as shown in Fig. 6, where the plots for the succeeding-layer scheme superiorly bound those for the adjacent scheme, over the various k . Note also that, while results on *EU-Air* are shown only for the ascendent layer ordering, by inverting this order we will have a switch between results corresponding to the inner asymmetric case with results corresponding to the outer asymmetric case. Moreover, Fig. 6(b) compares the effect of asymmetric inter-layer coupling on *Flickr* with and without time-awareness, for PMM solutions. Here we observe that both IC_{ia}^t and IC_{oa}^t plots are above those corresponding to IC_{ia} and IC_{oa} . This indicates that considering a smoothing term for the temporal distance between layers (Eq. (9)) leads to an increase in modularity. This general result is also confirmed by GL, LART and M-EMCD* (results not shown); for instance, GL achieved on *Flickr* modularity 0.462 for IC_{ia}^t , 0.468 for IC_{oa}^t , and 0.460 for IC_s^t , which compared to results shown in Table 7 represent increments in Q of 43%. Similarly, M-EMCD* obtained on *Flickr* modularity 0.975 for IC_{ia}^t , IC_{oa}^t , and IC_s^t , which is higher than the corresponding values reported in Table 9 for IC_a and IC_s , respectively.

Correlation analysis. Analogously to correlation analysis performed for the unordered case, we compare different settings of Q with selected statistics on topological properties. Figures 7 show results on *EU-Air* obtained by GL, LART, PMM and M-EMCD*, respectively. Again, for PMM, k was set to the number of communities corresponding to the best modularity performance achieved by the method.

As a general remark Q is always non-negatively correlated with all topological measures. More specifically, the correlation is highly positive with all measures, when GL is used, and with all measures but average path length and clustering coefficient, when LART and M-EMCD* are used; for PMM, correlation is very high with clustering coefficient, and mid-low with the other measures. When equipped with succeeding-layer coupling, correlation is higher than in the adjacent-layer setting with average path length (up to +0.14), node-set coverage (up to +0.02) and redundancy (up to +0.05) for the solution found by GL and M-EMCD*, and with average path length (up to +0.07), node-set coverage (up to +0.11) and edge-set coverage (up to +0.11) for the solution found by PMM. We also found that the layer ordering does not provide meaningful variations on the correlation values — plots regarding descendent layer ordering are reported in the *Appendix*.

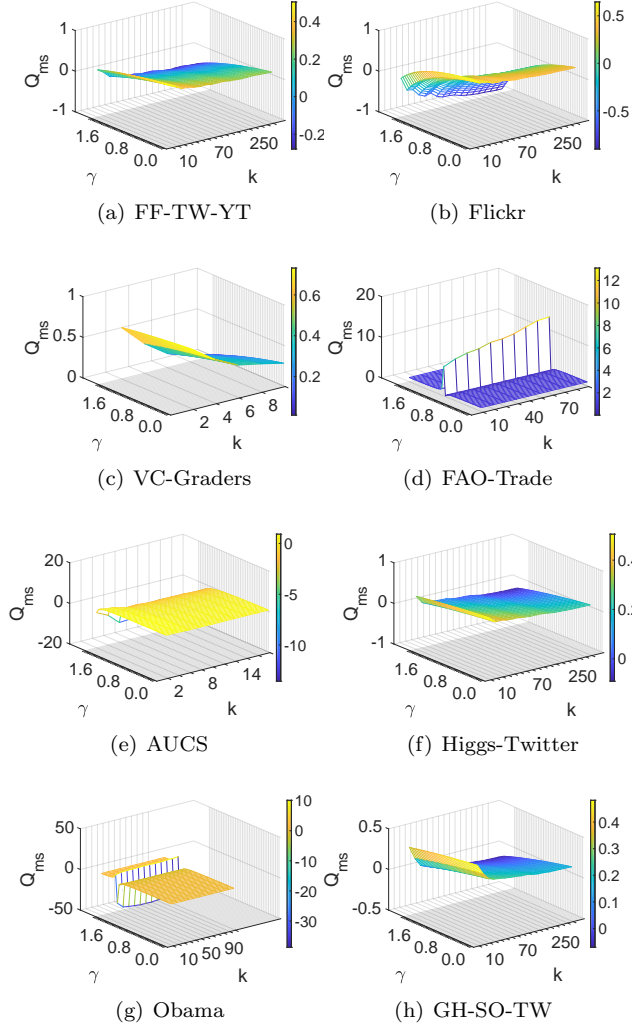


Figure 8: Mucha et al.’s modularity (Q_{ms}) by varying γ with $\omega = 1 - \gamma$

6.3 Analysis of Q_{ms} and comparison with Q

We discuss here performance results obtained by the community detection algorithms with Q_{ms} as assessment criterion. We will refer to the default setting of unordered set of layers as stated in [15].

Using GL, Q_{ms} tends to decrease as γ increases (while ω decreases, as it was varied with γ as $\omega = 1 - \gamma$). This occurs monotonically in most datasets, within positive ranges (e.g., from 0.636 to 0.384 on *FF-TW-YT*, from 0.525 to 0.391 on *GH-SO-TW*) or including negative modularity for higher γ (e.g., from 0.645

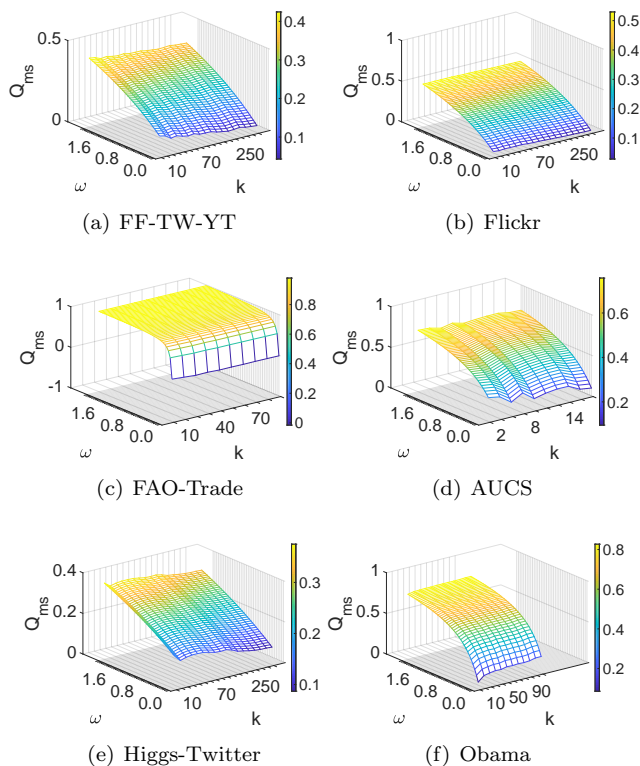


Figure 9: Mucha et al.’s modularity (Q_{ms}) by varying ω with $\gamma = 1$

to -0.05 on *Flickr*, from 0.854 to -4 on *AUCS*). Remarkably, the simultaneous effect of γ and $\omega = 1 - \gamma$ on Q_{ms} leads on some datasets (*Obama*, *EU-Air*, *London*) to a drastic degradation of modularity (down to much negative values) for some $\gamma > 1$, followed by a rapid increase to modularity of 1 as γ increases closely to 2. Analogous considerations hold for LART, PMM and M-EMCD*. For the latter method, the trend of drastic degradation of modularity followed by a rapid increase is only visible for *EU-Air*. For PMM, the plots of Fig. 8 show results by varying k , on the real-world datasets. Surprisingly, it appears that Q_{ms} is relatively less sensitive to the variation in the community structure than our Q . This is particularly visible in *AUCS*, *London* (not shown), and *Obama* where Q_{ms} shows no variation for increasing k . Also, it is worth noting that, for specific values of γ , Q_{ms} may have an abrupt decrease with very low peaks, as it happens for *Obama*. By contrast, for *FAO-Trade*, a value around 0.8 for γ induces high modularity which is stable for the different k values.

When varying ω within $[0.2]$, with $\gamma = 1$, Q_{ms} tends to monotonically increase as ω increases. This holds consistently on all datasets (Fig. 9 shows plots for some of them) with the only exception of *FAO-Trade*, where Q_{ms} is

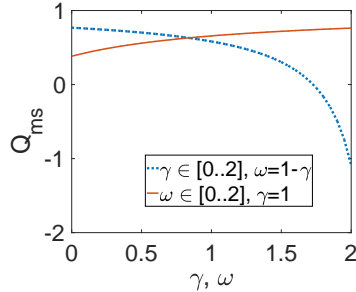


Figure 10: Mucha et al.’s modularity (Q_{ms}) by varying γ with $\omega = 1 - \gamma$ and by varying ω with $\gamma = 1$, on the ground-truth community structure of *AUCS*.

stable at 1 for $\omega > 0.8$. Variations are always on positive intervals (e.g., from 0.248 to 0.621 on *Flickr*, from 0.305 to 0.541 on *FF-TW-YT*, from 0.136 to 0.356 on *Higgs-Twitter*).

6.3.1 Comparison between Q and Q_{ms} : qualitative evaluation on the solutions generated by the community detection methods

In the light of the above analysis, a few interesting remarks arise by observing the different behavior of Q and Q_{ms} over the same community structure solutions, in function of the resolution and inter-layer coupling factors. From a qualitative viewpoint, the effect of ω on Q_{ms} turns out to be opposite, in most cases, to the effect of our *IC* terms on Q : that is, accounting more for the inter-layer couplings leads to increase Q_{ms} , while this does not necessarily happen in Q . Less straightforward is comparing the use of a constant resolution for all layers, as done in Q_{ms} , and the use of variable (i.e., for each pair of layer and community) resolutions, as done in Q . In this regard, we have previously observed that the use of a varying redundancy-based resolution factor improves Q w.r.t. the setting $\gamma = 1$. By coupling this general remark with the results (not shown) of an inspection of the values of $\gamma(L, C)$ in the computation of Q on the various network datasets (which confirmed that $\gamma(L, C)$ values span over its range, in practice), we can conclude that a more appropriate consideration of the term modeling the expected connectivity of community is realized in our Q w.r.t. keeping the resolution as constant for all layers in Q_{ms} .

6.3.2 Comparison between Q and Q_{ms} : evaluation on *AUCS* ground-truth communities

Let us now consider a further stage of evaluation of Q vs. Q_{ms} , which is complementary to the previous comparative analysis, with the specific purpose of assessing their behavior w.r.t. a *ground-truth community structure*. To this aim, we resorted again to the *AUCS* data: in their original work [43], the authors filled a gap in the literature (actually, still largely open) corresponding to a

lack of benchmarks for understanding multilayer/multiplex networks. In that work, the authors also provided a ground-truth multiplex community structure for *AUCS*, which reflects affiliation of the university employees/students to research groups. Please refer to [43] for a detailed description of how this ground-truth was obtained.

In this context of evaluation, we analyzed again the behaviors of Q and Q_{ms} under particular settings of the resolution and inter-layer coupling factors, while keeping fixed the community structure to a reference one corresponding to ground-truth knowledge. Before going into details of such analysis, let us first provide some remarks on the trends of Q_{ms} under its two settings previously considered in Sect. 6.3: varying γ within $[0..2]$ with $\omega = 1 - \gamma$, and varying ω within $[0..2]$ with $\gamma = 1$. As we observe from the results shown in Fig. 10, Q_{ms} can vary significantly depending on the setting of γ, ω : when $\gamma = 1, \omega \in [0..2]$, Q_{ms} monotonically increases with ω , varying within a relatively small range (i.e., from 0.38 to 0.76); however, when $\gamma \in [0..2], \omega = 1 - \gamma$, Q_{ms} follows an inverse trend, with a more rapid decrease for $\gamma > 1.5$, and overall wider range (from 0.768 to -1.09). Note that these considerations on the trends are consistent with the previous analysis for Q_{ms} computed on the solution found by PMM for *AUCS* (cf. Figs. 8–9 (e)). We shall come back later on such a high parameter-sensitivity of Q_{ms} .

Table 11 shows the global and community-specific values of Q and Q_{ms} for particular combinations of their corresponding γ and inter-layer coupling factors (IC and ω , respectively). Columns 2 to 5 report basic structural statistics for each of the communities, while the rest of the table is organized into three subtables: the first refers to Q_{ms} results, the second to our Q , and the third again to Q_{ms} with Q -biased settings of γ, ω . In the latter case, we wanted to make Q_{ms} “closer to” Q by setting its parameters to the values of $\gamma(L, C)$ and IC_s , respectively, averaged over the different communities and layers. Moreover, note that ground-truth communities in *AUCS* are 14 in total, however we only reported results for those (7) that contain more than one node, in order to avoid cluttering the table with roughly constant, zero-close modularity values that correspond to the singleton communities.

Looking at the table, communities C_2 and C_7 (resp. C_5, C_3 , and C_4) correspond to the highest (resp. lowest) modularity values, for either modularity measure, under each of the parameter-combinations considered. In general, beyond the differences in the respective values of modularity (note that Q_{ms} values still differ from the corresponding Q ones even for the Q -biased settings), the two measures appear to behave similarly over the various communities. To confirm this intuition, we evaluated the Pearson correlation of different pairings of Q and Q_{ms} community-specific values. Results show indeed almost perfect correlation (always above 0.98).

One aspect of evaluation that we also investigated is whether disrupting the multiplex network by layer may have effect on the comparison between Q and Q_{ms} , which resembles a sort of layer-oriented *resiliency* analysis. More specifically, based on the structural impact due to the various layers in *AUCS* [43], we considered the following alternative configurations: (i) we removed layer *co-*

Table 11: Comparison between specific settings of Q and Q_{ms} for each of the non-singleton ground-truth communities of $AUCS$

	#nodes/ #edges	avg. degree	avg. path length	clust. coeff.	Q_{ms}		Q				Q_{ms}				
					$\gamma = 1$		$\gamma = 1$		$\gamma(L, C)$		$\gamma = 1$		$\gamma = \text{avg } \gamma(L, C)$		
					$\omega = 1$	$\omega = 2$	IC_s	IC_{ia}	IC_s	IC_{ia}	IC_{ia}^{Adj}	IC_{ia}^{Suc}	$\omega = 1$	$\omega = \text{avg } IC_s$	$\omega = 1$
C_1	4/8	3.000	1.081	0.523	0.076	0.083	0.037	0.052	0.038	0.054	0.073	0.069	0.064	0.078	0.067
C_2	11/29	4.853	1.564	0.635	0.202	0.239	0.118	0.131	0.135	0.148	0.223	0.229	0.145	0.226	0.181
C_3	6/4	1.210	1.148	0.120	0.052	0.061	0.020	0.035	0.020	0.036	0.044	0.039	0.038	0.053	0.040
C_4	5/6	2.105	1.038	0.413	0.062	0.069	0.029	0.043	0.029	0.044	0.057	0.054	0.051	0.063	0.053
C_5	3/4	2.100	1.133	0.600	0.054	0.066	0.018	0.034	0.018	0.035	0.041	0.034	0.036	0.056	0.038
C_6	6/8	2.430	1.208	0.428	0.083	0.095	0.036	0.054	0.037	0.055	0.072	0.067	0.065	0.085	0.068
C_7	7/13	3.570	1.551	0.659	0.123	0.141	0.057	0.074	0.058	0.075	0.103	0.101	0.096	0.128	0.103
<i>Global modularity</i>					<i>0.651</i>	<i>0.754</i>	<i>0.314</i>	<i>0.424</i>	<i>0.337</i>	<i>0.447</i>	<i>0.615</i>	<i>0.593</i>	<i>0.495</i>	<i>0.689</i>	<i>0.550</i>

authorship (i.e., the smallest and less connected of all layers), (ii) we removed layers *co-authorship* and *leisure* (i.e., the ones having the lowest number of edges), (iii) we removed layer *work* (i.e., the one with the most edges), (iv) we retained layers *work* and *lunch* only. For each of such multiplex-disruption configurations, we replicated the above analysis corresponding to the full multiplex. Results (not shown) indicated no particular differences in terms of rankings of community modularity obtained by Q_{ms} and Q , respectively; however, we also observed a general decrease in Pearson correlation of the pairings of Q_{ms} and Q community-specific values, although the correlation remained still high, in particular always above 0.96 (e.g., when removing layer *work*, correlation was 0.965 between Q_{ms} with $\gamma = 1, \omega = \text{avg } IC_s$ and Q with $\gamma = 1, IC_s$, and 0.98 between Q_{ms} with $\gamma = \text{avg } \gamma(L, C), \omega = \text{avg } IC_s$ and Q with varying $\gamma(L, C), IC_s$).

To sum up, in this ground-truth evaluation, Q_{ms} and Q exhibited consistently similar behaviors at community level for specific settings of their respective parameters of resolution and inter-layer coupling. However, it should be emphasized that such a similarity between the two modularity values was actually achieved for either canonical settings of γ, ω in Q_{ms} (i.e., $\gamma = 1$ and $\omega \in \{1, 2\}$) or Q -biased settings of γ, ω (i.e., $\gamma = \text{avg } \gamma(L, C), \omega = \text{avg } IC_s$). In general, Q_{ms} has shown to be highly sensitive to the settings of its parameters, whereas by contrast, our Q has the key advantage of automatically determining the resolution and inter-layer coupling factors based on the structural information of the communities in the multilayer network.

6.4 Efficiency evaluation

We analyzed the computation time of Q for the different combinations of redundancy-based resolution factor γ and inter-layer coupling factors IC . The 3-D plots in Figs. 11–12 display the time vs. the number of layers and the number of nodes per layer. For this analysis, we referred to the solutions found by GL for the multilayer networks generated through the LFR benchmark (cf. Section 5.1.2).

As expected, the computation time increases with both the number of layers and nodes per layer, with the latter being less evident when setting γ fixed to 1. Also, while it is obvious that the computation time is higher when using variable (i.e., redundancy-based) resolution factor than in the case $\gamma = 1$ (with percentage increase of 50%, for the maximum number of layers and nodes per layer), we observe much less fluctuations in the plot surfaces than in the case of resolution factor fixed to 1, regardless of the setting of inter-layer coupling factors. The reader is also referred to the **Appendix** for further results by varying the inter-layer coupling settings.

7 Conclusion

We proposed a new definition of modularity for multilayer networks. Motivated by the opportunity of revising the multislice modularity proposed in [15], we

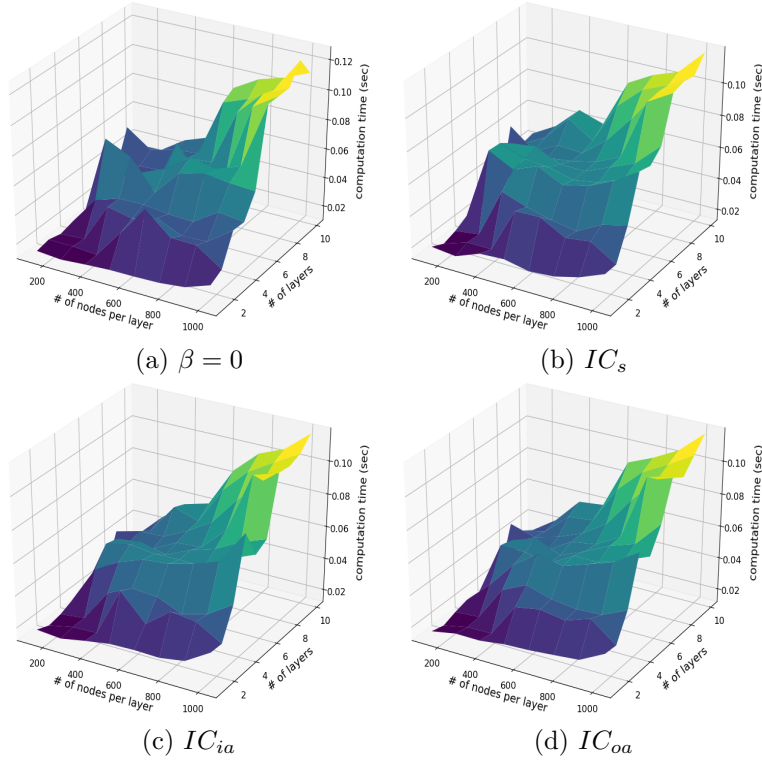


Figure 11: Computation time (in seconds) of the multilayer modularity Q , with $\gamma = 1$, measured on the solution found by GL on the multiplex LFR network

conceived alternative notions of layer resolution and inter-layer coupling, which are key-enabling for generalizations of modularity for multilayer networks. Using four state-of-the-art methods for multilayer community detection, synthetic multilayer networks and ten real-world multilayer networks, we provided empirical evidence of the significance of our proposed modularity.

Our work paves the way for the development of new optimization methods of community detection in multilayer networks which, by embedding our multilayer modularity, can discover community structures having the interesting properties relating to the proposed per-layer/community redundancy-based resolution factors and projection-based inter-layer coupling schemes. In this respect, we point out that our multilayer modularity is able to cope with communities that are overlapping at entity level, which eventually reflect the different roles that the same entity can play when occurring in two or more layers of the network. Within this view, one benefit of adopting the multilayer network model is that the problem of computing soft community-memberships of entities can be translated into a simpler problem of identification of crisp community-memberships of nodes within each layer. Nonetheless, a further interesting direction would

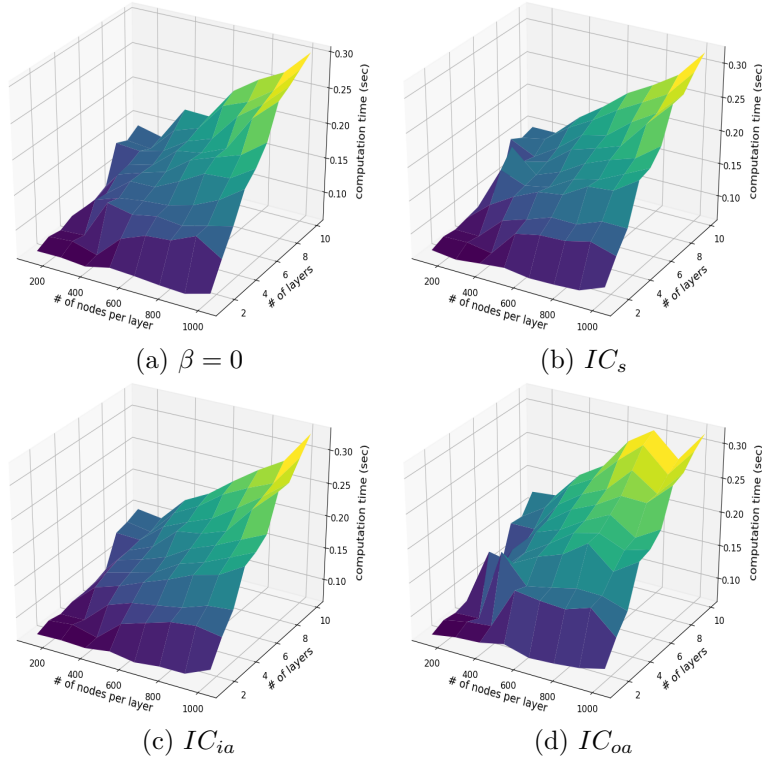


Figure 12: Computation time (in seconds) of the multilayer modularity Q , with redundancy-based $\gamma(L, C)$, measured on the solution found by GL on the multiplex LFR network

be to evaluate our multilayer modularity in contexts of node-overlapping communities. In this case, however, one challenge to face is whether and to what extent an overlapping-aware multilayer modularity should be able to measure the community overlaps within each layer and/or across the layers. Along this direction, it would be interesting to study an integration of our multilayer modularity into recently developed works that propose probabilistic representations or stochastic generative models for overlapping community detection in multilayer networks [49, 50].

Acknowledgements

This research work has been partly supported by the Start-(H)Open POR Grant No. J28C17000380006 funded by the Calabria Region Administration, and by the NextShop PON Grant No. F/050374/01-03/X32 funded by the Italian Ministry for Economic Development.

References

- [1] A. Amelio and A. Tagarelli, “Revisiting Resolution and Inter-Layer Coupling Factors in Modularity for Multilayer Networks,” in *Proc. IEEE/ACM ASONAM*, 2017, pp. 266–273.
- [2] M. E. J. Newman and M. Girvan, “Finding and evaluating community structure in networks,” *Phys. Rev. E*, vol. 69, no. 2, p. 026113, 2004.
- [3] M. E. J. Newman, “Fast algorithm for detecting community structure in networks,” *Phys. Rev. E*, vol. 69, 2004.
- [4] U. Brandes, D. Delling, M. Gaertler, R. Görke, M. Hoefer, Z. Nikoloski, and D. Wagner, “On modularity clustering,” *IEEE Trans. Knowl. Data Eng.*, vol. 20, no. 2, pp. 172–188, 2008.
- [5] M. Chen, K. Kuzmin, and B. K. Szymanski, “Community detection via maximization of modularity and its variants,” *IEEE Trans. Comput. Social Syst.*, vol. 1, no. 1, pp. 46–65, 2014.
- [6] A. Clauset, M. E. J. Newman, and C. Moore, “Finding community structure in very large networks,” *Phys. Rev. E*, vol. 70, 2004.
- [7] M. E. J. Newman, “Modularity and community structure in networks,” *Proc. Natl. Acad. Sci.*, pp. 8577–8582, 2005.
- [8] S. White and P. Smyth, “A spectral clustering approach to finding communities in graph,” in *Proc. SDM*, 2005.
- [9] J. Reichardt and S. Bornholdt, “Statistical mechanics of community detection,” *Phys. Rev. E*, vol. 74, 2006.
- [10] J. Duch and A. Arenas, “Community detection in complex networks using extremal optimization,” *Phys. Rev. E*, vol. 72, 2005.
- [11] S. Boccaletti, G. Bianconi, R. Criado, C. I. del Genio, J. G.-G. nes, M. Romance, I. S. na Nadal, Z. Wang, and M. Zanin, “The structure and dynamics of multilayer networks,” *Phys. Rep.*, vol. 544, no. 1, pp. 1–122, 2014.
- [12] M. E. Dickison, M. Magnani, and L. Rossi, *Multilayer social networks*. Cambridge University Press, 2016.
- [13] M. Kivela, A. Arenas, M. Barthelemy, J. P. Gleeson, Y. Moreno, and M. A. Porter, “Multilayer networks,” *J. Complex Netw.*, vol. 2, no. 3, pp. 203–271, 2014.
- [14] L. G. A. Alves, G. Mangioni, F. A. Rodrigues, P. Panzarasa, and Y. Moreno, “Unfolding the complexity of the global value chain: Strength and entropy in the single-layer, multiplex, and multi-layer international trade networks,” *Entropy*, vol. 20, no. 12, 2018.

- [15] P. J. Mucha, T. Richardson, K. Macon, M. A. Porter, and J.-P. Onnela, “Community structure in time-dependent, multiscale, and multiplex networks,” *Science*, vol. 328, no. 5980, pp. 876–878, 2010.
- [16] M. Coscia, F. Giannotti, and D. Pedreschi, “A classification for community discovery methods in complex networks,” *Stat. Anal. Data Min.*, vol. 4, no. 5, pp. 512–546, 2011.
- [17] Z. Kuncheva and G. Montana, “Community detection in multiplex networks using locally adaptive random walks,” in *Proc. IEEE/ACM ASONAM*, 2015, pp. 1308–1315.
- [18] H. Zhang, C. Wang, J. Lai, and P. S. Yu, “Modularity in Complex Multilayer Networks with Multiple Aspects: A Static Perspective,” *CoRR*, vol. abs/1605.06190, 2016.
- [19] A. Tagarelli, A. Amelio, and F. Gullo, “Ensemble-based community detection in multilayer networks,” *Data Min. Knowl. Discov.*, vol. 31, no. 5, pp. 1506–1543, 2017.
- [20] D. Mandaglio, A. Amelio, and A. Tagarelli, “Consensus Community Detection in Multilayer Networks Using Parameter-Free Graph Pruning,” in *Proc. PAKDD*, 2018, pp. 193–205.
- [21] S. Torreggiani, G. Mangioni, M. J. Puma, and G. Fagiolo, “Identifying the community structure of the food-trade international multi-network,” *Environ. Res. Lett.*, vol. 13, no. 5, p. 054026, 2018.
- [22] G. Mangioni, G. Jurman, and M. De Domenico, “Multilayer flows in molecular networks identify biological modules in the human proteome,” *IEEE Trans. Netw. Sci. Eng.*, 2018.
- [23] L. G. Alves, G. Mangioni, I. Cingolani, F. A. Rodrigues, P. Panzarasa, and Y. Moreno, “The nested structural organization of the worldwide trade multi-layer network,” *Sci. Rep.*, vol. 9, no. 1, p. 2866, 2019.
- [24] S. Fortunato and M. Barthelemy, “Resolution limit in community detection,” *Proc. Natl. Acad. Sci.*, vol. 104, no. 36, 2007.
- [25] S. Fortunato, “Community detection in graphs,” *Phys. Rep.*, vol. 486, no. 3, pp. 75–174, 2010.
- [26] L. Tang and H. Liu, *Community Detection and Mining in Social Media*, ser. Synthesis Lectures on Data Mining and Knowledge Discovery. Morgan & Claypool Publishers, 2010.
- [27] S. Fortunato and D. Hric, “Community detection in networks: A user guide,” *Phys. Rep.*, vol. 659, pp. 1–44, 2016.
- [28] E. A. Leicht and M. E. J. Newman, “Community structure in directed networks,” *Phys. Rev. Lett.*, vol. 100, p. 118703, Mar 2008.

- [29] A. Arenas, J. Duch, A. Fernández, and S. Gómez, “Size reduction of complex networks preserving modularity,” *New J. Phys.*, vol. 9, no. 6, p. 176, 2007.
- [30] M. E. J. Newman, “Analysis of weighted networks,” *Phys. Rev. E*, vol. 70, p. 056131, Nov 2004.
- [31] J. Xiang and K. Hu, “Limitation of multi-resolution methods in community detection,” *Physica A Stat. Mech. Appl.*, vol. 391, no. 20, pp. 4995–5003, 2012.
- [32] J. Zhang, K. Zhang, X. ke Xu, C. K. Tse, and M. Small, “Seeding the kernels in graphs: toward multi-resolution community analysis,” *New J. Phys.*, vol. 11, no. 11, p. 113003, 2009.
- [33] A. Arenas, A. Fernández, and S. Gómez, “Analysis of the structure of complex networks at different resolution levels,” *New J. Phys.*, vol. 10, no. 5, p. 053039, 2008.
- [34] J. Xiang, Y.-N. Tang, Y.-Y. Gao, Y. Zhang, K. Deng, X.-K. Xu, and K. Hu, “Multi-resolution community detection based on generalized self-loop rescaling strategy,” *Physica A Stat. Mech. Appl.*, vol. 432, pp. 127–139, 2015.
- [35] S. Gómez, P. Jensen, and A. Arenas, “Analysis of community structure in networks of correlated data,” *Phys. Rev. E*, vol. 80, p. 016114, 2009.
- [36] V. A. Traag and J. Bruggeman, “Community detection in networks with positive and negative links,” *Phys. Rev. E*, vol. 80, p. 036115, Sep 2009.
- [37] M. J. Barber, “Modularity and community detection in bipartite networks,” *Phys. Rev. E*, vol. 76, p. 066102, 2007.
- [38] Y. Xu, L. Chen, and S. Zou, “Community detection from bipartite networks,” in *Proc. IEEE WISA*, 2013, pp. 249–254.
- [39] R. Guimerà, M. Sales-Pardo, and L. A. N. Amaral, “Module identification in bipartite and directed networks,” *Phys. Rev. E*, vol. 76, p. 036102, 2007.
- [40] V. Nicosia, G. Mangioni, V. Carchiolo, and M. Malgeri, “Extending the definition of modularity to directed graphs with overlapping communities,” *J. Stat. Mech.*, vol. 2009, no. 03, p. P03024, 2009.
- [41] M. Berlingerio, M. Coscia, and F. Giannotti, “Finding and characterizing communities in multidimensional networks,” in *Proc. IEEE/ACM ASONAM*, 2011, pp. 490–494.
- [42] J. Kim and J. Lee, “Community detection in multi-layer graphs: A survey,” *SIGMOD Record*, vol. 44, no. 3, pp. 37–48, 2015.

- [43] L. Rossi and M. Magnani, “Towards effective visual analytics on multiplex and multilayer networks,” *Chaos, Solitons & Fractals*, vol. 72, pp. 68–76, 2015.
- [44] M. De Domenico, V. Nicosia, A. Arenas, and V. Latora, “Structural reducibility of multilayer networks,” *Nat. Commun.*, vol. 6, p. 6864, 2015.
- [45] M. Cha, A. Mislove, and K. P. Gummadi, “A Measurement-driven Analysis of Information Propagation in the Flickr Social Network,” in *Proc. WWW*, 2009, pp. 721–730.
- [46] G. Silvestri, J. Yang, A. Bozzon, and A. Tagarelli, “Linking accounts across social networks: the case of stackoverflow, github and twitter,” in *Proc. Work. on Knowl. Discov. on the Web*, 2015, pp. 41–52.
- [47] E. Omodei, M. De Domenico, and A. Arenas, “Characterizing interactions in online social networks during exceptional events,” *Frontiers in Physics*, vol. 3, p. 59, 2015.
- [48] L. Tang, X. Wang, and H. Liu, “Uncovering groups via heterogeneous interaction analysis,” in *Proc. IEEE ICDM*, 2009, pp. 503–512.
- [49] N. Stanley, S. Shai, D. Taylor, and P. J. Mucha, “Clustering network layers with the strata multilayer stochastic block model,” *IEEE Trans. Netw. Sci. Eng.*, vol. 3, no. 2, pp. 95–105, April 2016.
- [50] H. T. Ali, S. Liu, Y. Yilmaz, R. Couillet, I. Rajapakse, and A. O. Hero, “Latent heterogeneous multilayer community detection,” in *Proc. ICASSP*, 2019.

Appendix

A Analytical derivation of lower and upper bounds

Proof of Proposition 1 (Lower bound of Q). Let us assume that each of the ℓ layer graphs in $G_{\mathcal{L}}$ has the form of a bipartite graph $K_i(a, b)$, with $i = 1, \dots, \ell$, and sets a and b induce a partitioning of the set of nodes in two communities denoted as C_1 and C_2 , respectively, so that $\mathcal{C} = \{C_1, C_2\}$ with $|C_1| = |C_2| = \frac{n}{2}$, and no internal links are drawn between nodes of the same community (because of the bipartite assumption).

To begin with, consider the reduction of Q to its simplest form, i.e., $\gamma(L, C)$ fixed to 1 for any L, C and $\beta = 0$. Therefore, the contribution of community C_1 to Q is:

$$Q(C_1) = - \sum_{L \in \mathcal{L}} \left(\frac{d_L(C_1)}{d(V_{\mathcal{L}})} \right)^2.$$

Since $d_L(C_1) = \frac{n^2}{4}$ and $d(V_{\mathcal{L}}) = \frac{n^2}{4}(2\ell) = \frac{n^2\ell}{2}$, $Q(C_1)$ is calculated as:

$$Q(C_1) = - \sum_{L \in \mathcal{L}} \left(\frac{\frac{n^2}{4}}{\frac{n^2\ell}{2}} \right)^2 = -\frac{1}{4\ell}.$$

The same above holds for C_2 . Therefore, the minimum value of Q when $\gamma(L, C) = 1$ and $\beta = 0$ is as follows:

$$Q(\mathcal{C}) = -\frac{1}{4\ell}2 = -\frac{1}{2\ell}. \quad (14)$$

Let us now consider Q with its redundancy-based resolution factor while keeping $\beta = 0$. Since the internal degree of community C_1 is 0, there are no redundant pairs for any community and layer, and hence $\gamma(L, C) = 2$. Consequently, the contribution of C_1 to Q is:

$$Q(C_1) = -2 \sum_{L \in \mathcal{L}} \left(\frac{d_L(C_1)}{d(V_{\mathcal{L}})} \right)^2 = -2 \sum_{L \in \mathcal{L}} \left(\frac{1}{2\ell} \right)^2 = -\frac{1}{2\ell}.$$

The same above holds for C_2 . Therefore, the lower bound of Q when $\gamma(L, C)$ is variable and $\beta = 0$ is as follows:

$$Q(\mathcal{C}) = -\frac{1}{2\ell}2 = -\frac{1}{\ell}. \quad (15)$$

In the general form of Q with both resolution and inter-layer coupling factors (i.e., varying γ and $\beta = 1$), the contribution of C_1 to Q is:

$$Q(C_1) = \sum_{L \in \mathcal{L}} \left[-2 \left(\frac{d_L(C_1)}{d(V_{\mathcal{L}})} \right)^2 + \sum_{L' \in \mathcal{P}(L)} \frac{IC(C_1, L, L')}{d(V_{\mathcal{L}})} \right].$$

In the above formula, let us indicate the terms $X(C_1) = \sum_{L \in \mathcal{L}} -2 \left(\frac{d_L(C_1)}{d(V_{\mathcal{L}})} \right)^2$, and $Y(C_1) = \sum_{L \in \mathcal{L}, L' \in \mathcal{P}(L)} \frac{IC(C_1, L, L')}{d(V_{\mathcal{L}})}$. If we denote with $p = \sum_{L \in \mathcal{L}} |\mathcal{P}(L)|$ the total number of valid layer-pairings, then $d(V_{\mathcal{L}}) = \frac{n^2 \ell}{2} + np$, and $X(C_1)$ can be rewritten as follows:

$$X(C_1) = -2 \sum_{L \in \mathcal{L}} \left(\frac{\frac{n^2}{4}}{\frac{n^2 \ell}{2} + np} \right)^2 = -\frac{1}{2} \frac{n^2 \ell}{(n\ell + 2p)^2}.$$

For the reduction of the term $Y(C_1)$, we consider the two cases of symmetric inter-layer coupling and asymmetric inter-layer coupling. In the first case, the minimum value for $IC_s(C_1, L_i, L_j)$ is equal to $\frac{|C_1^{(i)} \cap C_1^{(j)}|}{|V_i \cap V_j|} = \frac{1}{n}$. Accordingly, $Y(C_1)$ is reduced as follows:

$$Y(C_1) = \sum_{L \in \mathcal{L}} \sum_{L' \in \mathcal{P}(L)} \frac{\frac{1}{n}}{\frac{n^2 \ell}{2} + np} = \frac{2p}{n^2(n\ell + 2p)}$$

In the second case, $IC_a(C_1, L_i, L_j) = \frac{|C_1^{(i)} \cap C_1^{(j)}|}{|V_i \cap V_j|} \times \frac{|V_i|}{|C_1^{(i)}|} = \frac{1}{n} \times \frac{n}{\frac{n}{2}} = \frac{2}{n}$. Accordingly, $Y(C_1)$ is reduced as follows:

$$Y(C_1) = \sum_{L \in \mathcal{L}} \sum_{L' \in \mathcal{P}(L)} \frac{\frac{2}{n}}{\frac{n^2 \ell}{2} + np} = \frac{4p}{n^2(n\ell + 2p)}.$$

The above expressions for X and Y hold for C_2 . Therefore, the lower bound of Q in its general form is as follows:

$$\begin{aligned} Q(C) &= 2(X(C_1) + Y(C_1)) = \\ &= -\frac{n^2 \ell}{(n\ell + 2p)^2} + \frac{4(1 + \eta)p}{n^2(n\ell + 2p)}, \end{aligned} \quad (16)$$

with $\eta = 0$ for IC_s and $\eta = 1$ for IC_a .

It should be noted that Eq. 15 is a special case of Eq. 16 with $\beta = 0$ and $d(V_{\mathcal{L}})$ discarding the contribution given by the inter-layer edges (i.e., $d(V_{\mathcal{L}}) = \frac{n^2 \ell}{2}$).

Proof of Proposition 2 (Upper bound of Q). Let us assume that each of the ℓ layer graphs in $G_{\mathcal{L}}$ has community structure $\mathcal{C} = \{C_1, C_2\}$ such that $|C_1| = |C_2| = \frac{n}{2}$ and each community is a clique with $\frac{n}{2} \left(\frac{n}{2} - 1 \right)$ edges. Moreover, there are no external edges connecting the communities, therefore $d_L(C) = d_L^{int}(C)$. Note that by uniformly distributing the n nodes into the two communities, it can easily be shown that the maximum of Q is higher.

Analogously to the analysis of the minimum value of Q , let us first consider the setting $\gamma(L, C) = 1$, for any L, C , and $\beta = 0$. Therefore, the contribution of community C_1 to Q is:

$$Q(C_1) = \sum_{L \in \mathcal{L}} \frac{d_L^{int}(C_1)}{d(V_{\mathcal{L}})} - \left(\frac{d_L^{int}(C_1)}{d(V_{\mathcal{L}})} \right)^2.$$

Because $d_L^{int}(C_1) = \frac{n}{2}(\frac{n}{2} - 1)$ and $d_L(\mathcal{V}) = \frac{n}{2}(\frac{n}{2} - 1)2\ell$, the above expression is rewritten as:

$$Q(C_1) = \sum_{L \in \mathcal{L}} \frac{\frac{n}{2}(\frac{n}{2} - 1)}{\frac{n}{2}(\frac{n}{2} - 1)2\ell} - \left(\frac{\frac{n}{2}(\frac{n}{2} - 1)}{\frac{n}{2}(\frac{n}{2} - 1)2\ell} \right)^2 = \frac{1}{2} - \frac{1}{4\ell}.$$

The same above holds for C_2 . Therefore, the maximum of Q when $\gamma(L, C) = 1$ and $\beta = 0$ is as follows:¹

$$Q(\mathcal{C}) = 2 \left(\frac{1}{2} - \frac{1}{4\ell} \right) = 1 - \frac{1}{2\ell} = \frac{2\ell - 1}{2\ell}. \quad (17)$$

Consider now the setting with redundancy-based $\gamma(L, C)$ and $\beta = 0$. The contribution of C_1 to Q is calculated as:

$$Q(C_1) = \sum_{L \in \mathcal{L}} \frac{\frac{n}{2}(\frac{n}{2} - 1)}{\frac{n}{2}(\frac{n}{2} - 1)2\ell} - \gamma(L, C_1) \left(\frac{\frac{n}{2}(\frac{n}{2} - 1)}{\frac{n}{2}(\frac{n}{2} - 1)2\ell} \right)^2.$$

Since $nnp(L, C_1) = \frac{\frac{n}{2}(\frac{n}{2} - 1)}{2}$, it follows that $\gamma(L, C_1)$ is equal to $2(1 + \log_2(1 + \frac{\frac{n}{2}(\frac{n}{2} - 1)}{2}))^{-1}$ for each layer and community. Note that the above constant quantity, hereinafter denoted as γ , tends to be $\ll 1$, and it is smaller for higher number of nodes n . The contribution of C_1 to Q is rewritten as:

$$Q(C_1) = \frac{1}{2} - \gamma \frac{1}{4\ell}.$$

The same above holds for C_2 . Therefore, the maximum of Q with redundancy-based $\gamma(L, C)$ and $\beta = 0$ is as follows:

$$Q(\mathcal{C}) = 2 \left[\frac{1}{2} - \gamma \frac{1}{4\ell} \right] = 1 - \gamma \frac{1}{2\ell} = \frac{2\ell - \gamma}{2\ell}. \quad (18)$$

Note that the above quantity is as much closer to 1 as n and ℓ are higher.

In the general setting of Q with redundancy-based $\gamma(L, C)$ and $\beta = 1$, the contribution of C_1 to Q is:

$$Q(C_1) = \sum_{L \in \mathcal{L}} \left[\frac{d_L^{int}(C_1)}{d(V_{\mathcal{L}})} - \gamma(L, C) \left(\frac{d_L^{int}(C_1)}{d(V_{\mathcal{L}})} \right)^2 + \sum_{L' \in \mathcal{P}(L)} \frac{IC(C_1, L, L')}{d(V_{\mathcal{L}})} \right].$$

In the above formula, let us indicate the terms $X(C_1) = \sum_{L \in \mathcal{L}} \left[\frac{d_L^{int}(C_1)}{d(V_{\mathcal{L}})} - \gamma(L, C) \left(\frac{d_L^{int}(C_1)}{d(V_{\mathcal{L}})} \right)^2 \right]$, and $Y(C_1) = \sum_{L \in \mathcal{L}} \sum_{L' \in \mathcal{P}(L)} \frac{IC(C_1, L, L')}{d(V_{\mathcal{L}})}$. Because $d_L^{int}(C_1) =$

¹If C_1 and C_2 would have $n - 1$ and 1 nodes, respectively, the resulting maximum value of Q will be $\frac{\ell - 1}{\ell}$, hence lower than what we obtain in Eq. 17.

$\frac{n}{2}(\frac{n}{2}-1)$, $d_L(\mathcal{V}) = \frac{n}{2}(\frac{n}{2}-1)2\ell + np$, and $\gamma(L, C_1) = 2(1 + \log_2(1 + \frac{\frac{n}{2}(\frac{n}{2}-1)}{2}))^{-1}$ for each layer and community, we obtain:

$$\begin{aligned} X(C_1) &= \sum_{L \in \mathcal{L}} \frac{\frac{n}{2}(\frac{n}{2}-1)}{\frac{n}{2}(\frac{n}{2}-1)2\ell + np} - \gamma \left(\frac{\frac{n}{2}(\frac{n}{2}-1)}{\frac{n}{2}(\frac{n}{2}-1)2\ell + np} \right)^2 \\ &= \frac{1}{2} \frac{(\frac{n}{2}-1)\ell}{(\frac{n}{2}-1)\ell + p} - \gamma \ell \left(\frac{1}{2} \frac{(\frac{n}{2}-1)}{(\frac{n}{2}-1)\ell + p} \right)^2, \\ Y(C_1) &= \sum_{L \in \mathcal{L}} \sum_{L' \in \mathcal{P}(L)} \frac{IC(C_1, L, L')}{\frac{n}{2}(\frac{n}{2}-1)2\ell + np}. \end{aligned}$$

For the reduction of the term $Y(C_1)$, we again consider the two cases of symmetric inter-layer coupling and asymmetric inter-layer coupling. In the first case, $IC_s(C_1, L_i, L_j) = \frac{|C_1^{(i)} \cap C_1^{(j)}|}{|V_i \cap V_j|} = \frac{1}{n}$. Therefore:

$$Y(C_1) = \sum_{L \in \mathcal{L}} \sum_{L' \in \mathcal{P}(L)} \frac{\frac{1}{n}}{n(\frac{n}{2}-1)\ell + np} = \frac{p}{n^2(\frac{n}{2}-1)\ell + n^2p}.$$

In the second case, $IC_a(C_1, L_i, L_j) = \frac{|C_1^{(i)} \cap C_1^{(j)}|}{|V_i \cap V_j|} \times \frac{|V_i|}{|C_1^{(i)}|} = \frac{1}{n} \times \frac{n}{\frac{n}{2}} = \frac{2}{n}$. Therefore:

$$Y(C_1) = \sum_{L \in \mathcal{L}} \sum_{L' \in \mathcal{P}(L)} \frac{\frac{2}{n}}{\frac{n}{2}(\frac{n}{2}-1)2\ell + np} = \frac{2p}{n^2(\frac{n}{2}-1)\ell + n^2p}.$$

The same above holds for C_2 . Therefore, the maximum value of Q is as follows:

$$\begin{aligned} Q(\mathcal{C}) &= 2(X(C_1) + Y(C_1)) = \\ &= 2 \left[\frac{1}{2} \frac{(\frac{n}{2}-1)\ell}{(\frac{n}{2}-1)\ell + p} - \gamma \ell \left(\frac{1}{2} \frac{(\frac{n}{2}-1)}{(\frac{n}{2}-1)\ell + p} \right)^2 + \right. \\ &\quad \left. + \frac{(1+\eta)p}{n^2(\frac{n}{2}-1)\ell + n^2p} \right] \end{aligned} \quad (19)$$

with $\eta = 0$ for IC_s and $\eta = 1$ for IC_a .

It is worth noting that Eq. 18 is a special case of Eq. 19 with $\beta = 0$ and $d(V_{\mathcal{L}})$ discarding the contribution given by the inter-layer edges.

B Evaluation with ordered layers

Figure 13 provides further details on correlation analysis using descendent layer ordering.

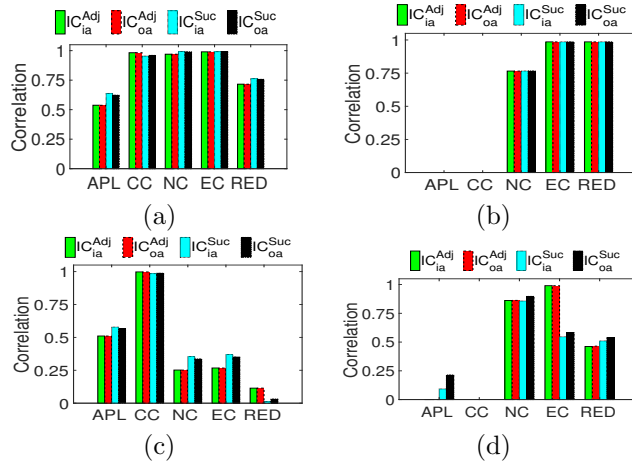


Figure 13: Pearson correlation coefficient between average path length (APL), clustering coefficient (CC), node coverage (NC), edge coverage (EC), redundancy (RED), and the multilayer modularity Q with $\gamma(L, C)$ and IC_{ia}^{Adj} , IC_{oa}^{Adj} , IC_{ia}^{Suc} , IC_{oa}^{Suc} , and descendent layer ordering, computed on the solution found by (a) GL, (b) LART, (c) PMM, and (d) M-EMCD* on the *EU-Air* network. Each statistics is computed at community-level

C Efficiency results

Figures 14–15 show the computation time of Q for the different combinations of γ and IC factors.

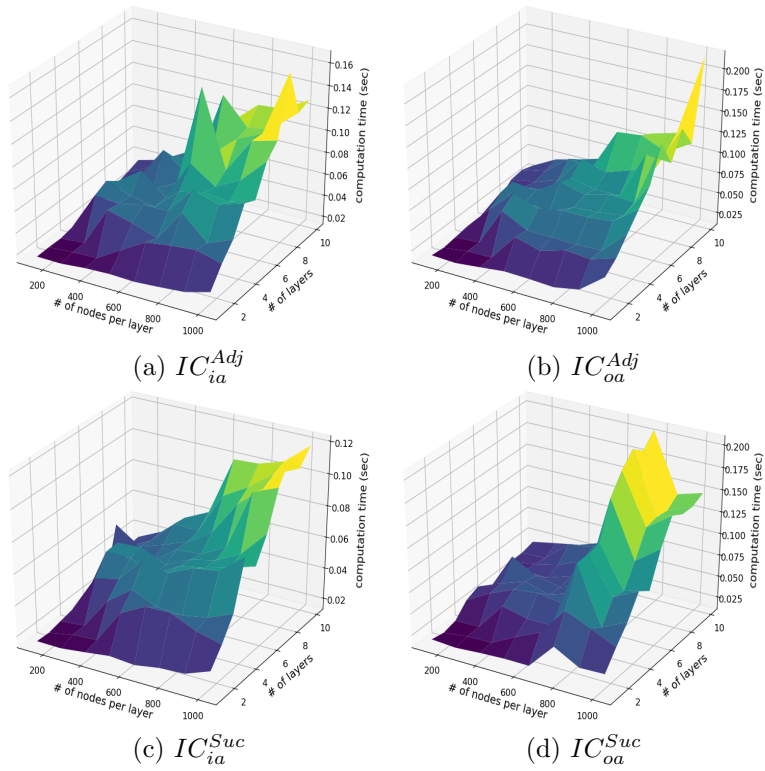


Figure 14: Computation time (in seconds) of the multilayer modularity Q , with $\gamma = 1$, measured on the solution found by GL on the multiplex LFR network

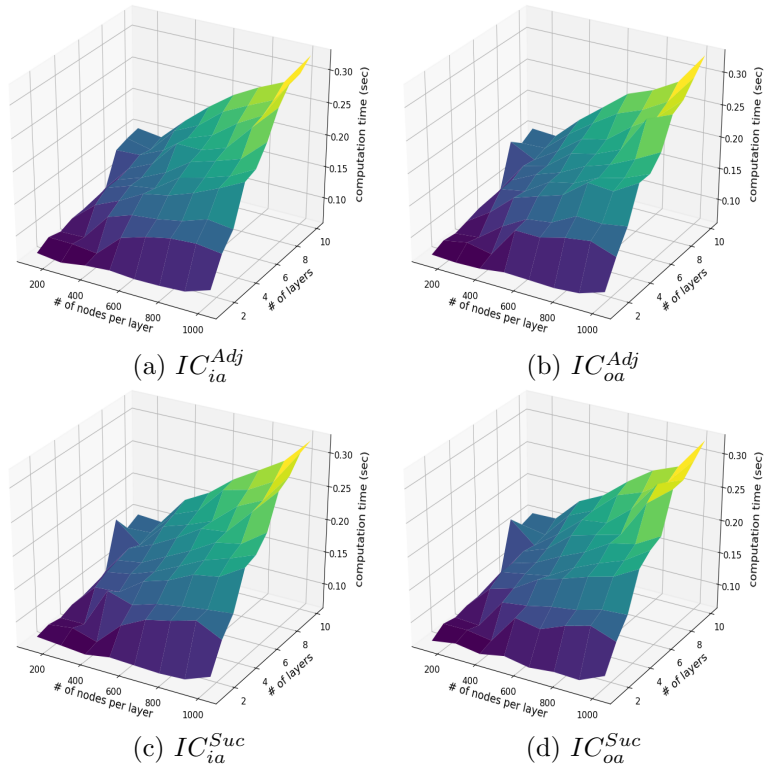


Figure 15: Computation time (in seconds) of the multilayer modularity Q , with redundancy-based $\gamma(L, C)$, measured on the solution found by GL on the multiplex LFR network